Title :
ORCHIDEE MICT-LEAK (r5459), a global model for the production, transport and transformation of dissolved organic carbon from Arctic permafrost regions, Part 1: Rationale, model description and simulation protocol.

Authors:
S.P.K. Bowring[1], R. Lauerwald[2], B. Guenet[1], D. Zhu[1], M. Guimberteau[1,3], A. Tootchi[3], A. Ducharne[3], P. Ciais[1]

Affiliations:
[1] Laboratoire des Sciences du Climat et de l'Environnement, LSCE, CEA, CNRS, UVSQ, 91191 Gif Sur Yvette, France
[2] Department of Geoscience, Environment & Society, Université Libre de Bruxelles, 1050 Bruxelles, Belgium
[3] Sorbonne Université, CNRS, EPHE, Milieux environnementaux, transferts et interaction dans les hydrosystèmes et les sols, Metis, 75005 Paris, France

Abstract
Few Earth System models adequately represent the unique permafrost soil biogeochemistry and its respective processes; this significantly contributes to uncertainty in estimating their responses, and that of the planet at large, to warming. Likewise, the riverine component of what is known as the 'boundless carbon cycle' is seldom recognised in Earth System modelling. Hydrological mobilisation of organic material from a ~1330–1580 PgC carbon stock to the river network results either in sedimentary settling or atmospheric 'evasion', processes widely expected to increase with amplified Arctic climate warming. Here, the production, transport and atmospheric release of dissolved organic carbon (DOC) from high-latitude permafrost soils into inland waters and the ocean is explicitly represented for the first time in the land surface component (ORCHIDEE) of a CMIP6 global climate model (Institut Pierre Simon Laplace (IPSL)). The model, ORCHIDEE MICT-LEAK, which represents the merger of previously described ORCHIDEE versions -MICT and -LEAK, mechanistically represents (a) vegetation and soil physical processes for high latitude snow, ice and soil phenomena, and (b) the cycling of DOC and CO_2, including atmospheric evasion, along the terrestrial-aquatic continuum from soils through the river network to the coast, at 0.5° to 2° resolution. This paper, the first in a two-part study, presents the rationale for including these processes in a high latitude specific land surface model, then describes the model with a focus on novel process implementations, followed by a summary of the model configuration and simulation protocol. The results of these simulation runs, conducted for the Lena River basin, are evaluated against observational data in the second part of this study.

1 Introduction

High-latitude permafrost soils contain large stores of frozen, often ancient and relatively reactive carbon up to depths of over 30m. Soil warming caused by contemporary anthropogenic climate change can be expected to destabilise these stores (Schuur et al., 2015) via microbial or hydrological mobilisation following spring/summer thaw and riverine discharge (Vonk et al., 2015a) as the boundary between discontinuous and continuous permafrost migrates poleward and toward the continental interior over

50 time. The high latitude soil carbon reservoir may amount to ~1330–1580 PgC
51 (Hugelius et al., 2013, 2014; Tarnocai et al., 2009) –over double that stored in the
52 contemporary atmosphere, while the yearly lateral flux of carbon from soils to running
53 waters may amount to about a fifth of net ecosystem carbon exchange (~400 TgC yr^{-1}),
54 about ~40% of which may be contributed by DOC (McGuire et al., 2009). Excluding the
55 dissolved inorganic carbon component of this flux, as well as dissolved CO_2 input from
56 soils, the vast majority (85%) of riverine organic carbon transfer to the Arctic Ocean
57 occurs as dissolved organic carbon (DOC), as described in (e.g.) Suzuki et al. (2006)..

59 The fact that, to our knowledge, no existing land surface models are able to adequately
60 simultaneously represent this unique high latitude permafrost soil environment, the
61 transformation of soil organic carbon (SOC) to its eroded particulate and DOC forms and
62 their subsequent lateral transport, as well as the response of all these to warming,
63 entails significant additional uncertainty in projecting global-scale biogeochemical
64 responses to human-induced environmental change.

66 Fundamental to these efforts is the ability to predict the medium under which carbon
67 transformation will occur: in the soil, streams, rivers or sea, and under what
68 metabolising conditions –since these will determine the process mix that will ultimately
69 enable either terrestrial redeposition and retention, ocean transfer, or atmospheric
70 release of permafrost-derived organic carbon. In the permafrost context, this implies
71 being able to accurately represent (i) the source, reactivity and transformation of
72 released organic matter, and; (ii) the dynamic response of hydrological processes to
73 warming, since water phase determines carbon, heat, and soil moisture availability for
74 metabolisation and lateral transport.

76 For this purpose, we take a specific version of the terrestrial component of the Institut
77 Pierre Simon Laplace (IPSL) global Earth System model (ESM) ORCHIDEE (Organising
78 Carbon and Hydrology In Dynamic Ecosystems), one that is specifically coded for,
79 calibrated with and evaluated on high latitude phenomena and permafrost processes,
80 called ORCHIDEE-MICT (where MICT stands for aMeliorated Interactions between
81 Carbon and Temperature (Guimberteau et al., 2018)). This code is then adapted to
82 include DOC production in the soil (ORCHIDEE-SOM, (Camino-Serrano et al., 2018)),
83 'priming' of SOC (ORCHIDEE-PRIM,(Guenet et al., 2016, 2018)) and the riverine
84 transport of DOC and CO_2, including in-stream transformations, carbon and water
85 exchanges with wetland soils and gaseous exchange between river surfaces and the
86 atmosphere (ORCHILEAK (Lauerwald et al., 2017), where the suffix 'LEAK' holds no
87 acronym, and refers to the 'leakage' of carbon from terrestrial to aquatic realms).

89 The resulting model, dubbed ORCHIDEE MICT-LEAK, hereafter referred to as MICT-L for
90 brevity, is therefore able to represent: (a) Permafrost soil and snow physics,
91 thermodynamics to a depth of 38m and dynamic soil hydrology to a depth of 2m; (b)
92 Improved representation of biotic stress response to cold, heat and moisture in high
93 latitudes; (c) Explicit representation of the active layer and frozen-soil hydrologic
94 barriers; buildup of soil carbon stocks via primary production and vertical translocation
95 (turbation) of SOC and DOC; (d) DOC leaching from tree canopies, atmospheric
96 deposition, litter and soil organic matter, its adsorption/desorption to/from soil
97 particles, its transport and transformation to dissolved CO_2 ($CO^*_{2(aq.)}$) and atmospheric
98 release, as well as the production and hydrological transport of plant root-zone derived

99   dissolved CO_2; (e) Improved representation of C cycling on floodplains; (f) Priming of
100 organic matter in the soil column and subsequent decomposition dynamics.   In
101 combination, these model properties allow us to explore the possibility of reproducing
102 important emergent phenomena observed in recent empirical studies (Fig. 1) arising
103 from the interaction of a broad combination of different processes and factors.
104
105 To our knowledge very few attempts have been made at the global scale of modelling
106 DOC production and lateral transfer from the permafrost region that explicitly accounts
107 for such a broad range of high latitude–specific processes, which in turn allows us to
108 match and evaluate simulation outputs with specific observed processes, enhancing our
109 ability to interpret the output from theses models and improve our understanding of the
110 processes represented. The only other attempt at doing so is a Pan-Arctic modelling
111 study by Kicklighter et al. (2013), which is based on a relatively simplified scheme for
112 soil, water and biology. The following segment briefly overviews the dynamics,
113 emergent properties and their overall significance across scales, of permafrost region
114 river basins.
115
116 ***A giant, reactive, fast-draining funnel: A permafrost basin overview***
117
118 Permafrost has a profound impact on Arctic river hydrology. In permafrost regions, a
119 permanently frozen soil layer acts as a 'cap' on ground water flow (see 'permafrost
120 barrier', right hand side of Fig. 1). This implies that: (i) Near-surface runoff becomes by
121 far the dominant flowpath draining permafrost watersheds (Ye et al., 2009), as shown
122 in Fig. 1d; (ii) The seasonal amplitude of river discharge, expressed by the ratio of
123 maximum to minimum discharge ($Q_{max:min}$ in Fig. 1), over continuous versus
124 discontinuous permafrost catchments is higher as a result of the permafrost barrier;
125 (iii) This concentration of water volume near the surface causes intense leaching of DOC
126 from litter and relevant unfrozen soil layers (Fig. 1g, 1d, e.g. Suzuki et al., (2006) Drake
127 et al., (2015) ; Spencer et al., (2015); (Vonk et al., (2015a,b)); (iv) Permafrost SOC stocks
128 beneath the active layer are physically and thermally shielded from aquatic mobilisation
129 and metabolisation, respectively (Fig. 1g).
130
131 Rapid melting of snow and soil or river ice during spring freshet (May-June) drives
132 intensely seasonal discharge, with peaks often two orders of magnitude (e.g. Van Vliet et
133 al., (2012)) above baseflow rates (Fig. 1d). These events are the cause of four, largely
134 synchronous processes: (i) Biogenic matter is rapidly transported from elevated
135 headwater catchments (Fig. 1, right hand side) (McClelland et al., 2016); (ii) Plant
136 material at the soil surface is intensely leached, with subsequent mobilisation and
137 transformation of this dissolved matter via inland waters (Fig. 1d,b,j); During spring
138 freshet, riverine DOC concentrations increase and bulk annual marine DOC exports are
139 dominated by the terrestrial DOC flux to the rivers that occurs at this time (Holmes et al.,
140 2012). Indeed, DOC concentrations during the thawing season tend to be greater than
141 or equal to those in the Amazon particularly in the flatter Eurasian rivers (Holmes et al.,
142 2012; McClelland et al., 2012), and DOC concentrations are affected at watershed scale
143 by parent material, ground ice content (O'Donnell et al., 2016) and active layer depth
144 (Suzuki et al., 2006).
145
146 (iii) Sudden inundation of the floodplain regions in spring and early summer (Fig. 1h),
147 (Smith and Pavelsky, 2008), further spurs lateral flux of both particulate and dissolved

148 matter in the process and its re-deposition (Zubrzycki et al., 2013) or atmospheric
149 evasion (Fig. 1j,m); (iv) Snowmelt-induced soil water saturation, favouring the growth of
150 moss and sedge-based ecosystems (e.g. Selvam et al., 2017; Tarnocai et al., 2009; Yu,
151 2011) and the retention of their organic matter (OM),.i.e., peat formation, not shown in
152 Fig. 1 as this isn't represented in this model version, but is generated in a separate
153 branch of ORCHIDEE (Qiu et al., 2018)).

155 Mid-summer river low-flow and a deeper active layer allow for the hydrological
156 intrusion and leaching of older soil horizons (e.g. the top part of Pleistocene-era Yedoma
157 soils), and their subsequent dissolved transport (e.g. Wickland et al., 2018). These
158 sometimes-ancient low molecular weight carbon compounds appear to be preferentially
159 and rapidly metabolised by microbes in headwater streams (Fig. 1j), which may
160 constitute a significant fraction of aggregate summer CO_2 evasion in Arctic rivers
161 (Denfeld et al., 2013; Vonk et al., 2015). This is likely due to the existence of a significant
162 labile component of frozen carbon (Drake et al., 2015; Vonk et al., 2013; Woods et al.,
163 2011);

165 CO_2 evasion rates from Arctic inland waters (Fig. 1j,e,m), which include both lakes and
166 rivers, are estimated to be 40-84 TgC yr^{-1} (McGuire et al., 2009), of which 15-30 TgC yr^{-1}
167 or one-third of the total inland evasion flux, is thought to come from rivers. Recent geo-
168 statistically determined estimates of boreal lake annual emissions alone now stands at
169 74-347 TgC yr^{-1} (Hastie et al., 2018), although this is likely a substantial overestimate
170 (Bogard et al., 2019), which potentially lowers the riverine fraction of total CO_2 evasion.
171 These numbers should be compared with estimates of Pan-Arctic DOC discharge from
172 rivers of 25-36 TgC yr^{-1}(Holmes et al., 2012; Raymond et al., 2007). The subsequent
173 influx of terrestrial carbon to the shelf zone is thought to total 45-54 TgC yr^{-1}. Rivers
174 supply the Arctic Ocean an estimated 34 Tg of carbon-equivalent DOC (DOC-C) yr^{-1}
175 (Holmes et al., 2012), while depositing 5.8 Tg yr^{-1} of particulate carbon, these being
176 sourced from those rivers draining low and high elevation headwaters, respectively
177 (McClelland et al., 2016). These dynamics are all subject to considerable amplification
178 by changes in temperature and hydrology (e.g. Drake et al., 2015; Frey and McClelland,
179 2009; Tank et al., 2018).

181 Average annual discharge in the Eurasian Arctic rivers has increased by at least 7%
182 between 1936-1999 (Peterson et al., 2002), driven by increasing temperatures and
183 runoff (Berezovskaya et al., 2005), and the subsequent interplay of increasing annual
184 precipitation, decreasing snow depth and snow water equivalent (SWE) mass (Kunkel et
185 al., 2016; Mudryk et al., 2015), and greater evapotranspiration (Suzuki et al., 2018;
186 Zhang et al., 2009). Although net discharge trend rates over N. America were negative
187 over the period 1964-2003, since 2003 they have been positive on average (Dery et al.,
188 2016). These dynamic and largely increasing hydrologic flux trends point towards
189 temperature and precipitation -driven changes in the soil column, in which increased
190 soil water/snow thaw and microbial activity (Graham et al., 2012; MacKelprang et al.,
191 2011; Schuur et al., 2009) converge to raise soil leaching and DOC export rates to the
192 river basin and beyond (e.g. Vonk et al., (2015b)). Further, microbial activity generates
193 its own heat, which incubation experiments have shown may be sufficient to
194 significantly warm the soil further (Hollesen et al., 2015), in a positive feedback.

195

196 Arctic region fire events are also on the rise and likely to increase with temperature and
197 severity over time (Ponomarev et al., 2016). The initial burning of biomass is
198 accompanied by active layer deepening, priming of deeper soil horizons (De Baets et al.,
199 2016), and a significant loading of pyrogenic DOC in Arctic watersheds, up to half of
200 which is rapidly metabolised (Myers-Pigg et al., 2015).
201
202 In these contexts, the implications of (polar-amplified) warmer temperatures leading to
203 active layer deepening towards the future (transition from Continuous to Discontinuous
204 Permafrost, as shown in the upper/lower segments of Fig. 1) are clear and unique:
205 potentially sizeable aquatic mobilisation and microbial metabolisation (Xue, 2017) of
206 dissolved and eroded OM, deeper hydrological flow paths, an increase in total carbon
207 and water mass and heat transfer to the aquatic network and, ultimately, the Arctic
208 Ocean and atmosphere (Fig. 1i).
209
210 The advantage of having a terrestrial model that can be coupled to a marine component
211 of an overarching global climate model (GCM) is in this case the representation of a
212 consistent transboundary scheme, such that output from one model is integrated as
213 input to another. This is particularly important given the context in which these
214 terrestrial outflows occur :
215
216 Because of its small size, a uniquely large and shallow continental shelf, the global
217 climatological significance of its seasonal sea ice (Rhein et al., 2013) and its rapid decline
218 (Findlay et al., 2015), the Arctic Ocean has been described as a giant estuary (McClelland
219 et al., 2012), acting as a funnel for the transport, processing and sedimentation of
220 terrestrial OM. Because of its small surface area and shallow seas (Jakobsson, 2002), the
221 Arctic Ocean holds relatively little volume and is consequently sensitive to inputs of
222 freshwater, heat, alkalinity and nutrients that flush out from terrestrial sources,
223 particularly at discharge peak.
224
225 High suspended particle loads in river water as they approach the mouth (Heim et al.,
226 2014) cause lower light availability and water albedo and hence higher temperatures
227 (Bauch et al., 2013; Janout et al., 2016), which can affect the near-shore sea ice extent,
228 particularly in spring (Steele and Ermold, 2015). Volumes of riverine freshwater and
229 total energy flux (Lammers et al., 2007) are expected to increase with warmer
230 temperatures, along with an earlier discharge peak (Van Vliet et al., 2012, 2013). In
231 doing so, freshwaters may in the future trigger earlier onset of ice retreat (Stroeve et al.,
232 2014; Whitefield et al., 2015) via a freshwater albedo, ice melt, seawater albedo, ice
233 melt, feedback, amplified by intermediary state variables such as water vapour and
234 cloudiness (Serreze and Barry, 2011).
235
236 Both terrestrially-exported and older shelf carbon in the Arctic Ocean face considerable
237 disruption (McGuire et al., 2009; Schuur et al., 2015) from the combined effects of
238 increased freshwater, heat, sediment, nutrient and organic carbon flows from rapidly
239 warming Arctic river watersheds, as well as those from melting sea ice, warmer marine
240 water temperatures and geothermal heat sources (Janout et al., 2016; Shakhova et al.,
241 2015). Because ORCHIDEE is a sub-component of the overarching IPSL ESM, there is
242 scope for coupling riverine outputs of water, DOC, $CO_{2(aq)}$ and heat from the terrestrial
243 model as input for the IPSL marine components (Fig. 1i). Nonetheless, these are not the
244 objectives of the present paper, whose aim is rather to validate the simulated variable

245 output produced by the model described in detail below against observations and
246 empirical knowledge for the Lena basin, but are included here descriptively to scope the
247 plausible future applications of ORCHIDEE MICT-LEAK, given our present empirical
248 understanding of their potential significance. The choice of the Lena River basin in
249 Eastern Siberia as the watershed of study for model evaluation owes itself to its size, the
250 presence of floodplains and mountain areas which allow us to test the model behavior
251 for contrasting topography, the relatively low impact of damming on the river, given that
252 ORCHIDEE only simulates undammed fluvial 'natural flow', and its mixture of
253 continuous and discontinuous permafrost with tundra grassland in the north and boreal
254 forests in the south, and is described in greater detail in Part 2 of this study.

256 The Methods section summarises the model structure and associated rationale for each
257 of the model sub-branches or routines relevant to this study, and follows with the setup
258 and rationale for the simulations carried out as validation exercises.

2 Methods

262 This section overviews the processes represented in the model being described in this
263 manuscript, which is referred to as ORCHIDEE MICT-LEAK, hereafter referred to MICT-L
264 for brevity. MICT-L is at its heart a merge of two distinct models : the high-latitude land
265 surface component of the IPSL Earth System Model ORCHIDEE MICT, and the DOC-
266 production and transport branch of ORCHIDEE's default or 'trunk' version (Krinner et
267 al., 2005), ORCHILEAK. The original merger of these two code sets was between
268 ORCHILEAK and ORCHIDEE-MICT, which are described in Camino-Serrano et al.
269 (2018)/Lauerwald et al. (2017) and Guimberteau et al. (2018), respectively.

271 However, numerous improvements in code performance and process additions post-
272 dating these publications have been included in this code. Furthermore, novel processes
273 included in neither of these two core models are added to MICT-L, such as the diffusion
274 of DOC through the soil column to represent its turbation and preferential stabilisation
275 at depth in the soil, as described in Section.2.11.

277 In terms of code architecture, the resulting model is substantially different from either
278 of its parents, owing to the fact that the two models were developed on the basis of
279 ORCHIDEE trunk revisions 2728 and 3976 for ORCHILEAK and MICT respectively, which
280 have a temporal model development distance of over 2 years, and subsequently evolved
281 in their own directions. These foundational differences, which mostly affect the
282 formulation of soil, carbon and hydrology schemes, mean that different aspects of each
283 are necessarily forced into the subsequent code. Where these differences were
284 considered scientific or code improvements, they were included in the resulting scheme.
285 Despite architectural novelties introduced, MICT-L carries with it a marriage of much
286 the same schemes detailed exhaustively in Guimberteau et al. (2018) and Lauerwald et
287 al. (2017). As such, the following model description details only new elements of the
288 model, those that are critical to the production and transport of DOC from permafrost
289 regions, and parameterisations specific to this study (Fig. 2).

2.1 Model Description

293 MICT-L is based largely on ORCHIDEE-MICT, into which the DOC production, transport

294 and transformation processes developed in the ORCHILEAK model version and tested
295 insofar only for the Amazon, have been transplanted, allowing for these same processes
296 to be generated in high latitude regions with permafrost soils and a river flow regime
297 dominated by snow melt.   The description that ensues roughly follows the order of the
298 carbon and water flow chain depicted in Fig. 2b.   At the heart of the scheme is the
299 vegetative production of carbon, which occurs along a spectrum of 13 plant functional
300 types (PFTs) that differ from one another in terms of plant physiological and
301 phenological uptake and release parameters (Krinner et al., 2005). Together, these
302 determine grid-scale net primary production.   In the northern high latitudes, the boreal
303 trees (PFTs 7-9) and C3 grasses (PFT 10) dominate landscape biomass and primary
304 production.   Thus, in descending order yearly primary production over the Lena basin is
305 roughly broken down between C3 grasses (48%), boreal needleleaf summergreen trees
306 (27%), boreal needleleaf evergreen trees (12%), boreal broadleaf summergreen trees
307 (8%) and temperate broad-leaved evergreen trees (6%).   Naturally these basin
308 aggregates are heterogeneously distributed along latitude and temperature contours,
309 with grasses/tundra dominating at the high latitudes and (e.g.) temperate broadleaf
310 trees existing only at the southern edges of the basin.
311
312 **2.2 Biomass generation** (Fig. 1a)
313
314 Biomass generation, consisting of foliage, roots, above and below –ground sap and heart
315 wood, carbon reserves and fruit pools in the model, results in the transfer of these
316 carbon stores to two downstream litter pools, the structural and metabolic litter (Figure
317 2b). This distinction, defined by lignin concentration of each biomass pool (Krinner et
318 al., 2005), separates the relatively reactive litter fraction such as leafy matter from its
319 less-reactive, recalcitrant counterpart (woody, 'structural' material), with the
320 consequence that the turnover time of the latter is roughly four-fold that of the former.
321 These two litter pools are further subdivided into above and below –ground pools, with
322 the latter explicitly discretised over the first two metres of the soil column, a feature first
323 introduced to the ORCHIDEE model by Camino-Serrano et al. (2014, 2018). This marks
324 a significant departure from the original litter formulation in ORCHIDEE-MICT, in which
325 the vertical distribution of litter influx to the soil carbon pool follows a prescribed root
326 profile for each PFT. This change now allows for the production of DOC from litter
327 explicitly at a given soil depth in permafrost soils.
328
329 **2.3 DOC generation and leaching** (Fig. 1b)
330
331 The vast majority of DOC produced by the model is generated initially from the litter
332 pools via decomposition, such that half of all of the decomposed litter is returned to the
333 atmosphere as CO_2, as defined by the microbial carbon use efficiency (CUE) –the fraction
334 of carbon assimilated versus respired by microbes post-consumption –here set at 0.5
335 following Manzoni et al. (2012). The non-respired half of the litter feeds into 'Active',
336 'Slow' and 'Passive' free DOC pools, which correspond to DOC reactivity classes in the
337 soil column in an analogous extension to the standard CENTURY formulation (Parton et
338 al., 1987).   Metabolic litter contributes exclusively to the Active DOC pool, while
339 Structural litter feeds into the other two, the distribution between them dependent on
340 the lignin content of the Structural litter. The reactive SOC pools then derive directly
341 from this DOC reservoir, in that fractions of each DOC pool, defined again by the CUE, are
342 directly transferred to three different SOC pools, while the remainder adds to the

heterotrophic soil respiration. Depending on clay content and bulk density of the soil, a fraction of DOC is adsorbed to the mineral soil and does not take part in these reactions until it is gradually desorbed when concentrations of free DOC decrease in the soil column. This scheme is explained in detail in Camino-Serrano (2018). The value of the fractional redistributions between free DOC and SOC after adsorption are shown in Fig. 2b.

The approximate ratio of relative residence times for the three SOC pools in our model (Active :Slow :Passive) is (1 :37:1618) at a soil temperature of 5°C, or 0.843 years, 31 yrs. and 1364 yrs. for the three pools respectively (Fig. 2b). These are based on our own exploratory model runs and subsequent calculations. The residence times of the active DOC pool is $\sim$7 days (0.02 yrs.), while the slow and passive DOC pools both have a residence time of $\sim$343 days (0.94 yrs.) at that same temperature. Upon microbial degradation in the model, SOC of each pool reverts either to DOC or to CO_2, the ratio between these determined again by the CUE which is set in this study at 0.5 for all donor pools, in keeping with the parameter configuration in Lauerwald et al., (2017) from Manzoni et al. (2012). This step in the chain of flows effectively represents leaching of SOC to DOC. Note that the reversion of SOC to DOC occurs only along Active-Active, Slow-Slow and Passive-Passive lines in Fig. 2b, while the conversion of DOC to SOC is distributed differently so as to build up a reasonable distribution of soil carbon stock reactivities. Note also that the microbial CUE is invoked twice in the chain of carbon breakdown, meaning that the 'effective' CUE of the SOC-litter system is approximately 0.25.

2.4 Throughfall and its DOC (Fig. 1c)

In MICT-L, DOC generation also occurs in the form of wet and dry atmospheric deposition and canopy exudation, collectively attributed to the throughfall, i.e. the amount of precipitation reaching the ground. Wet atmospheric deposition originates from organic compounds dispersed in atmospheric moisture which become deposited within rainfall, and are assumed here to maintain a constant concentration. This concentration we take from the average of reported rainfall DOC concentrations in the empirical literature measured at sites >55°N (Bergkvist and Folkeson, 1992; Clarke et al., 2007; Fröberg et al., 2006; Lindroos et al., 2011; Rosenqvist et al., 2010; Starr et al., 2003; Wu et al., 2010), whose value is 3 mgC L^{-1} of rainfall. Dry DOC deposition occurs through aerosol-bound organic compounds, here assumed to fall on the canopy ; canopy exudation refers to plant sugars exuded from the leaf surface (e.g. honey dew) or from their extraction by heterotrophs such as aphids. These two are lumped together in our estimates of canopy DOC generation (gDOC per g leaf carbon), which is calibrated as follows.

We take the average total observation-based throughfall DOC flux rate per m^2 of forest from the aforementioned literature bundle (15.7 gC m^{-2} yr^{-1}) and subtract from it the wet deposition component (product of rainfall over our simulation area and the rain DOC content). The remainder is then the canopy DOC, which we scale to the average leaf biomass simulated in a 107-year calibration run over the Lena river basin. From this we obtain a constant tree canopy DOC production rate of 9.2*10^{-4} g DOC-C per gram of leaf biomass per day (Eq. 1). This is the same for all PFTs except those representing crops, for which this value equals 0, reflecting how at a very general level, crops are small and

tend no to be characterised by high organic acid loss rates from leaves due to e.g. aphids, due to human control. Note that this production of DOC should be C initially fixed by photosynthesis, but it is here represented as an additional carbon flux. The dry deposition of DOC through the canopy is given by:

$$(1) \quad TF_{DRY} = M_{LEAF} * 9.2 * 10^{-4} \frac{dt}{day}$$

Where TF_{DRY} is dry deposition of DOC from the canopy, M_{LEAF} is leaf biomass, dt is the timestep of the surface hydrology and energy balance module (30min) and day is 24 hours. This accumulates in the canopy and can be flushed out with the throughfall and percolates into the soil surface or adds to the DOC stock of surface waters. The wet and canopy deposition which hits the soil is then assumed to be split evenly between the labile and refractory DOC pools (following Aitkenhead-Peterson et al., 2003).

2.5 Hydrological mobilisation of soil DOC (Fig. 1d)

All DOC pools, leached from the decomposition of either litter and SOC or being throughfall inputs, reside at this point in discrete layers within the soil column, but are now also available for vertical advection and diffusion, as well as lateral export from the soil column as a carbon tracer, via soil drainage and runoff.

Export of DOC from the soil to rivers occurs through surface runoff, soil-bottom drainage, or flooding events (see section 2.8, 'Representation of floodplain hydrology and their DOC budget'). Runoff is activated when the maximum water infiltration rate of the specific soil has been exceeded, meaning that water arrives at the soil surface faster than it can enter, forcing it to be transported laterally across the surface. DOC is drawn up into this runoff water flux from the first 5 layers of the soil column, which correspond to a cumulative source depth of 4.5cm.

Drainage of DOC occurs first as its advection between the discrete soil layers, and its subsequent export from the 11th layer, which represents the bottom of the first 2m of the soil column, from which export is calculated as a proportion of the DOC concentration at this layer. Below this, soil moisture and DOC concentrations are no longer explicitly calculated, except in the case that they are cryoturbated below this, up to a depth of 3m. DOC drainage is proportional to but not a constant multiplier of the water drainage rate for two reasons. First, as it water percolates through the soil column, it carries DOC along from one layer to another through the entirety of the soil column, but this percolation is blocked when the soil is entirely frozen, i.e. it is assumed that all soil pores are filled with ice which blocks percolation. This implies that DOC transport is not just determined by what enters from the top but also by the below ground production from litter, the sorption and de-sorption to and from particulate soil organic carbon in the soil column, , its decomposition within the soil column, and water vertical transport entraining DOC between the non-frozen soil layers using the hydraulic conductivity calculated by the model as a function of soil texture, soil carbon and time-dependent soil moisture (Guimberteau et al., 2018).

438 Secondly, in order to account for preferential flow paths in the soil created by the
439 subsoil actions of flora and fauna, and for the existence of non-homogenous soil textures
440 at depth that act as aquitards, DOC infiltration must account for the fact that area-
441 aggregated soils drain more slowly, increasing the residence time of DOC in the soil.
442 Thus a reduction factor which reduces the vertical advection of DOC in soil solution by
443 80% compared to the advection is applied to represent a slow down in DOC percolation
444 through the soil and increase its residence time there.
445
446 In MICT-L, as in ORCHILEAK, a 'poor soils' module reads off from a map giving fractional
447 coverage of land underlain by Podzols and Arenosols at the 0.5° grid-scale, as derived
448 from the Harmonized World Soil Database (Nachtergaele, 2010). Due to their low pH
449 and nutrient levels, areas identified by this soil-type criterion experience soil organic
450 matter decomposition rates half that of other soils (Lauerwald et al. (2017), derived
451 from Bardy et al. (2011); Vitousek & Sanford (1986); Vitousek & Hobbie (2000)). To
452 account for the very low DOC-filtering capacity of these coarse-grained, base- and clay-
453 poor soils (DeLuca & Boisvenue (2012), Fig. 2b), no reduction factor in DOC advection
454 rate relative to that of water in the soil column is applied when DOC is generated within
455 these "poor soils".
456
457 By regulating both decomposition and soil moisture flux, the "poor soil" criterion
458 effectively serves a similar if not equal function to a soil 'tile' for DOC infiltration in the
459 soil column (inset box of Fig. 1), because soil tiles (forest, grassland/tundra/cropland
460 and bare soil) are determinants of soil hydrology which affects moisture-limited
461 decomposition. Here however, the 'poor soil' criteria is applied uniformly across the
462 three soil tiles of each grid cell. This modulation in MICT-L is of significance for the
463 Arctic region, given that large fractions of the discontinuous permafrost region are
464 underlain by Podzols, particularly in Eurasia. For the Arctic as a whole, Podzols cover
465 ~15% of total surface area (DeLuca and Boisvenue, 2012). Further, in modelled frozen
466 soils, a sharp decline in hydraulic conductivity is imposed by the physical barrier of ice
467 filling the soil pores, which retards the flow of water to depth in the soil, imposing a cap
468 on drainage and thus potentially increasing runoff of water laterally, across the soil
469 surface (Gouttevin et al., 2012). In doing so, frozen soil layers overlain by liquid soil
470 moisture will experience enhanced residence times of water in the carbon-rich upper
471 soil layers, potentially enriching their DOC load.   Note that ice wedges, an important
472 component of permafrost landscapes and their thaw processes, are not included in the
473 current terrestrial representation, but have been previously simulated in other models
474 (Lee et al., 2014).
475
476 Thus, for all the soil layers in the first 2m, DOC stocks are controlled by production from
477 litter and SOC decay, their advection, diffusion, and consumption by DOC mineralisation,
478 as well as buffering by adsorption and desorption processes.
479
480 **2.6 Routing Scheme:**
481
482 The routing scheme in ORCHIDEE, first described in detail in Ngo-Duc et al. (2007) and
483 presented after some version iterations in Guimberteau et al. (2012), is the module
484 which when activated, represents the transport of water collected by the runoff and
485 drainage simulated by the model along the prescribed river network in a given
486 watershed. In doing so, its purpose is to coarsely represent the hydrologic coupling

487 between precipitation inputs to the model and subsequent terrestrial runoff and
488 drainage (or evaporation) calculated by it on the one hand, and the eventual discharge of
489 freshwater to the marine domain, on the other. In other words, the routing scheme
490 simulates the transport of water by rivers and streams, by connecting rainfall and
491 continental river discharge with the land surface.
492
493 To do so, the routing scheme first inputs a map of global watersheds at the 0.5 degree
494 scale (Oki et al., 1999; Vorosmarty et al., 2000) which gives watershed and sub-basin
495 boundaries and the direction of water-flow based on topography to the model. The
496 water flows themselves are comprised of three distinct linear reservoirs within each
497 sub-basin ('slow', 'fast', 'stream'). Each water reservoir is represented at the   scale
498 (here: 4 sub-grid units per grid cell), and updated with the lateral in- and outflows at a
499 daily time-step. The 'slow' water reservoir aggregates the soil drainage, i.e. the vertical
500 outflow from the 11th layer (2 m depth) of the soil column, effectively representing
501 'shallow groundwater' transport and storage. The 'fast' water reservoir aggregates
502 surface runoff simulated in the model, effectively representing overland hydrologic flow.
503 The 'fast' water reservoir aggregates surface runoff simulated in the model, effectively
504 representing overland hydrologic flow. The 'slow' and 'fast' water reservoirs feed a
505 delayed outflow to the 'stream' reservoir' of the next downstream sub-grid quadrant
506
507 The water residence time in each reservoir depends on the nature of the reservoir
508 (increasing residence time in the order: stream < fast < slow reservoir). More generally,
509 residence time locally decreases with topographic slope and the grid-cell length, used as
510 a proxy for the main tributary length (Ducharne et al., 2003; Guimberteau et al., 2012).
511 This is done to reproduce the hydrological effects of geomorphological and topographic
512 factors in Manning's equation (Manning, 1891) and determines the time that water and
513 DOC remain in soils prior to entering the river network or groundwater. In this way the
514 runoff and drainage are exported from sub-unit to sub-unit and from grid-cell to grid-
515 cell.
516
517
518 **2.7 Grid-scale water and carbon routing** (Fig. 1f, 1g)
519
520
521 Water-borne, terrestrially-derived DOC and dissolved CO_2 in the soil solution are
522 exported over the land surface using the same routing scheme.   When exported from
523 soil or litter, DOC remains differentiated in the numerical simulations according to its
524 initial reactivity within the soil (Active, Slow, Passive). However, because the terrestrial
525 Slow and Passive DOC pools (Camino-Serrano et al., 2018) are given the same residence
526 time, these two pools are merged when exported (Lauerwald et al., 2017): Active DOC
527 flows into a Labile DOC hydrological export pool, while the Slow and Passive DOC pools
528 flow into a Refractory DOC hydrological pool (Fig. 2b), owing to the fact that the
529 residence time of these latter soil DOC pools is the same in their original (ORCHIDEE-
530 SOM) formulation (Camino-Serrano et al., 2018), and retained and merged into a single
531 hydrological DOC pool in Lauerwald et al. (2017). The water residence times in each
532 reservoir of each sub-grid scale quadrant determine the decomposition of DOC into CO_2
533 within water reservoirs, before non-decomposed DOC is passed on to the next reservoir
534 in the downstream sub-grid quadrant.
535

536 The river routing calculations, which occur at a daily timestep, are then aggregated to
537 one-day for the lateral transfer of water, $CO_{2(aq)}$ and DOC from upstream grid to
538 downstream grid according to the river network. Note that carbonate chemistry in
539 rivers and total alkalinity routing are not calculated here.

541 In this framework, the 'fast' and 'slow' residence times of the water pools in the routing
542 scheme determine the time that water and DOC remains in overland and groundwater
543 flow before entering the river network. Note that while we do not explicitly simulate
544 headwaters as they exist in a geographically determinant way in the real world, we do
545 simulate what happens to the water before it flows into a water body large enough to be
546 represented in the routing scheme by the water pool called 'stream', representing a real-
547 world river of stream order 4 or higher. The 'fast' reservoir is thus the runoff water flow
548 that is destined for entering the 'stream' water reservoir, and implicitly represents
549 headwater streams of Strahler order 1 to 3 by filling the spatial and temporal niche
550 between overland runoff and the river stem. The dynamics of headwater hydrological
551 and DOC dynamics (Section 2.10) are of potentially great significance with respect to
552 carbon processing, as headwater catchments have been shown to be 'hotspots' of carbon
553 metabolisation and outgassing in Arctic rivers, despite their relatively small areal
554 fraction (Denfeld et al., 2013; Drake et al., 2015; Mann et al., 2015; Suzuki et al., 2006;
555 Venkiteswaran et al., 2014; Vonk et al., 2013, 2015a, 2015b). Thus, in what follows in
556 this study, we refer to what in the code are called the 'fast' and 'stream' pools, which
557 represent the small streams and large stream or river pools, respectively, using 'stream'
558 and 'river' to denote these from hereon in.

560 Furthermore, the differentiated representation of water pools as well as mean grid cell
561 slope, combined with the dynamic active layer simulated for continuous versus
562 discontinuous permafrost, is important for reproducing the phenomena observed by
563 Kutscher et al. (2017) and Zhang et al. (2017) for sloping land as shown on the right
564 hand side of Fig. 1. In discontinuous permafrost and permafrost free regions, these
565 phenomena encompass landscape processes (sub-grid in the model), through which
566 water flow is able to re-infiltrate the soil column and so leach more refractory DOC
567 deeper in the soil column, leading to a more refractory signal in the drainage waters. In
568 contrast, in continuous permafrost region, the shallow active layer will inhibit the
569 downward re-infiltration flux of water and encourage leaching at the more organic-rich
570 and labile surface soil layer, resulting in a more labile DOC signal from the drainage in
571 these areas (Fig. 1). In addition, places with higher elevation and slope in these regions
572 tend to experience extreme cold, leading to lower NPP and so DOC leaching. The re-
573 infiltration processes mentioned are thought to be accentuated in areas with higher
574 topographic relief (Jasechko et al., 2016), which is why they are represented on sloping
575 areas in Fig. 1.

577 **2.8 Representation of floodplain hydrology and their DOC budget** (Fig. 1e,1h)

579 The third terrestrial DOC export pathway in MICT-L is through flooding of floodplains, a
580 transient period that occurs when stream water is forced by high discharge rates over
581 the river 'banks' and flows onto a flat floodplain area of the grid cell that the river
582 crosses, thus inundating the soil. Such a floodplain area is represented as a fraction of a
583 grid-cell with the maximum extent of inundation, termed the 'potential flooded area'
584 being predefined from a forcing file (Tootchi et al., 2019). Here, the DOC pools that are

already being produced in these inundated areas from litter and SOC decomposition in the first 5 layers of the soil column are directly absorbed by the overlying flood waters. These flood waters may then either process the DOC directly, via oxidisation to CO_2, (Sections 2.10, 2.11) or return them to the river network, as floodwaters recede to the river main stem, at which point they join the runoff and drainage export flows from upstream.

MICT-L includes the floodplain hydrology part of the routing scheme (D'Orgeval et al., 2008; Guimberteau et al., 2012), as well as additions and improvements described in Lauerwald et al. (2017). The spatial areas that are available for potential flooding are pre-defined by an input map originally based on the map of Prigent et al. (2007). However, for this study, we used an alternative map of the "regularly flooded areas" derived from the method described in Tootchi et al., (2019), which in this study uses an improved input potential flooding area forcing file specific to the Lena basin, that combines three high-resolution surface water and inundation datasets derived from satellite imagery: GIEMS-D15 (Fluet-Chouinard et al., 2015), which results from the downscaling of the map of Prigent et al. (2007) at 15-arc-sec (ca 500 m at Equator); ESA-CCI land cover (at 300 m ~ 10 arc-sec); and JRC surface water at 1 arc-sec (Pekel et al., 2016). The 'fusion' approach followed by this forcing dataset stems from the assumption that the potential flooding areas identified by the different datasets are all valid despite their uncertainties, although none of them is exhaustive. The resulting map was constructed globally at the 15 arc-sec resolution and care was taken to exclude large permanent lakes from the potential flooding area based on the HydroLAKES database (Messager et al., 2016). In the Lena river basin, the basin against which we evaluate ORCHIDEE MICT-LEAK in Part 2 of this study, this new potential floodplains file gives a maximum floodable area of 12.1% ($2.4*10^5$ km^2) of the $2.5*10^6$ km^2 basin, substantially higher than previous estimates of 4.2% by Prigent et al. (2007).

With this improved forcing, river discharge becomes available to flood a specific pre-defined floodplain grid fraction, creating a temporary floodplains hydrologic reservoir, whose magnitude is defined by the excess of discharge at that point over a threshold value, given by the median simulated water storage of water in each grid cell over a 30 year period. The maximum extent of within-grid flooding is given by another threshold, the calculated height of flood waters beyond which it is assumed that the entire grid is inundated. This height, which used to be fixed at 2 m, is now determined by the 90th percentile of all flood water height levels calculated per grid cell from total water storage of that grid cell over a reference simulation period for the Lena basin, using the same methodology introduced by Lauerwald et al. (2017). The residence time of water on the floodplains (τ_{flood}) is a determinant of its resulting DOC concentration, since during this period it appropriates all DOC produced by the top 5 layers of the soil column.

2.9 Oceanic outflow (Fig. 1i)

Routing of water and DOC through the river network ultimately lead to their export from the terrestrial system at the river mouth (Fig. 1), which for high latitude rivers are almost entirely sub-deltas of the greater 'estuary', described by McClelland et al. (2012), draining into the Arctic Ocean. Otherwise, the only other loss pathway for carbon export once in the river network is through its decomposition to CO_2 and subsequent

634 escape to the atmosphere from the river surface. DOC decomposition is ascribed a
635 constant fraction for the labile and refractory DOC pools of 0.3 d^{-1} and 0.01 d^{-1} at 25°C,
636 respectively, these modulated by a water-temperature dependent Arrhenius rate term.
637 Because the concentration of dissolved CO_2 (referred to as $CO_{2(aq.)}$) in river water is
638 derived not only from in-stream decomposition of DOC, but also from $CO_{2(aq.)}$ inputs
639 from the decomposition of litter, SOC and DOC both in upland soils and in inundated
640 soils, the model also represents the lateral transport of $CO_{2(aq.)}$ from soils through the
641 river network. Note that autochtonous primary production and derivative carbon
642 transformations are ignored here, as they are considered relatively minor contributors
643 in the Arctic lateral flux system (Cauwet and Sidorov, 1996; Sorokin and Sorokin, 1996).
644
645 **2.10 Dissolved CO_2 export and river evasion** (Fig. 1j)
646
647 Soil $CO_{2(aq.)}$ exports are simulated by first assuming a constant concentration of $CO_{2(aq.)}$
648 with surface runoff and drainage water fluxes, of 20 and 2 mgC L^{-1}, corresponding to a
649 pCO2 of 50000 μatm and 5000 μatm at 25°C in the soil column, respectively. These
650 quantities are then scaled with total (root, microbial, litter) soil respiration by a scaling
651 factor first employed in Lauerwald et al. (2019, *in review*). In the high latitudes soil
652 respiration is dominantly controlled by microbial decomposition, and for the Lena basin
653 initial model tests suggest that its proportional contribution to total respiration is
654 roughly 90%, versus 10% from root respiration. Thus $CO_{2(aq.)}$ enters and circulates the
655 rivers via the same routing scheme as that for DOC and river water. The lateral transfers
656 of carbon are aggregated from the 30 minute time steps at which they are calculated,
657 with a 48 timestep period, so that they occur within the model as a daily flux. The
658 calculation of the river network pCO2 can then be made from $CO_{2(aq.)}$ and its equilibrium
659 with the atmosphere, which is a function of its solubility (K_{CO2}) with respect to the
660 temperature of the water surface T_{WATER} (Eq.2).
661

$$(2) \quad pCO_{2POOL} = \frac{[CO_{2(aq)}]}{12.011 * K_{CO_2}}$$

662
663 Where the pCO2 (atm.) of a given (e.g. 'stream', 'fast', 'slow' and floodplain) water pool
664 (pCO2POOL) is given by the dissolved CO_2 concentration in that pool $[CO_{2(aq)}]$, the molar
665 weight of carbon (12.011 g mol^{-1}) and K_{CO2}. Water temperature (T_{WATER}, (°C)) isn't
666 simulated by the model, but is derived here from the average daily surface temperature
667 (T_{GROUND}, (°C)) in the model (Eq. 3), a derivation calculated for ORCHIDEE by Lauerwald
668 et al. (2017) and retained here. Note that while dissolved CO_2 enters from the terrestrial
669 reservoir from organic matter decomposition, it is also generated *in situ* within the river
670 network as DOC is respired microbially.
671
672 With our water temperature estimate, both K_{CO2} and the Schmidt number (*Sc,* Eq. 4)
673 from Wanninkhof (1992) can be calculated, allowing for simulation of actual gas
674 exchange velocities from standard conditions. The Schmidt number links the gas
675 transfer velocity of any soluble gas (in this case carbon dioxide) from the water surface
676 to water temperature. For more on the Schmidt number see (Wanninkhof, 2014, 1992).
677 The CO_2 that evades is then subtracted from the $[CO_{2(aq)}]$ stocks of each of the different
678 hydrologic reservoirs –river, flood and stream.
679

$$(3) \quad T_{WATER} = 6.13°C + (0.8 * T_{GROUND})$$

$$(4) \; Sc = \big((1911 - 118.11) * T_{WATER}\big) + \big(3.453 * T_{WATER}^2\big) - \big(0.0413 * T_{WATER}^3\big)$$

681
682 CO_2 evasion is therefore assumed to originate from the interplay of CO_2 solubility,
683 relative gradient in partial pressures of CO_2 between air and water, and gas exchange
684 kinetics. Evasion as a flux from river and floodplain water surfaces is calculated at a
685 daily timestep, however in order to satisfy the sensitivity of the relative gradient of
686 partial pressures of CO_2 in the water column and atmosphere to both CO_2 inputs and
687 evasion, the pCO$_2$ of water is calculated at a more refined 6 minute timestep. The daily
688 lateral flux of CO_2 inputs to the water column are thus equally broken up into 240 (6
689 min.) segments per day and distributed to the pCO$_2$ calculation. Other relevant carbon
690 processing pathways, such as the photochemical breakdown of riverine dissolved
691 organic carbon, are not explicitly included here, despite the suggestion by some studies
692 that the photochemical pathway dominate DOC processing in Arctic streams (e.g. Cory et
693 al., 2014). Rather, these processes are bundled into the aggregate decomposition rates
694 used in the model, which thus include both microbial and photochemical oxidation. This
695 is largely because it is unclear how different factors contribute to breaking down DOC in
696 a dynamic environment and also the extent to which our DOC decomposition and CO_2
697 calculations implicitly include both pathways –e.g. to what extent the equations and
698 concepts used in their calculation confound bacterial with photochemical causation,
699 since both microbial activity and incident UV light are a function of temperature and
700 total incident light.
701
702 **2.11 Soil layer processes: turbation** (Fig. 1k), **adsorption** (Fig. 1l)
703
704 The soil carbon module is discretised into a 32-layer scheme totalling 38m depth, which
705 it shares with the soil thermodynamics to calculate temperature through the entire
706 column. An aboveground snow module (Wang et al., 2013) is discretised into 3 layers of
707 differing thickness, heat conductance and density, which collectively act as a
708 thermodynamically-insulating intermediary between soil and atmosphere (Fig. 2a).
709 Inputs to the three soil carbon pools are resolved only for the top 2m of the soil, where
710 litter and DOC are exchanged with SOC in decomposition and adsorption/desorption
711 processes. Decomposition of SOC pools, calculated in each soil layer, is dependent on
712 soil temperature, moisture and texture (Koven et al., 2009; Zhu et al., 2016), while
713 vertical transfer of SOC is enabled by representation of cryoturbation (downward
714 movement of matter due to repeated freeze-thaw) in permafrost regions, and
715 bioturbation (by soil organisms) in non-permafrost regions in terms of a diffusive flux.
716
717 Cryoturbation, given a diffusive mixing rate (Diff) of 0.001 m^2 yr^{-1} (Koven et al., 2009), is
718 possible to 3 m depth (diffusive rate declines linearly to zero from active layer bottom to
719 3 m), and extends the soil column carbon concentration depth in permafrost regions
720 from 2 m. Bioturbation is possible to 2 m depth, with a mixing rate of 0.0001 m^2 yr^{-1}
721 (Koven et al., 2013) declining to zero at 2 m (Eq. 5). In MICT-L, these vertical exchanges
722 in the soil column are improved on. Now, we explicitly include the cryoturbation and
723 bioturbation of both belowground litter and DOC. These were not possible in
724 ORCHIDEE-MICT because, for the former, the belowground litter distribution was not
725 explicitly discretised or vertically dynamic, and for the latter because DOC was not
726 produced in prior versions. Diffusion is given by :
727

$$((5) \quad \frac{\delta DOC_i(z)}{\delta t} = IN_{DOC_i}(z) - k_i(z) * \phi * DOC_i(z) + Diff\frac{\delta DOC_i^2(z)}{\delta z^2}$$

Where DOC_i is the DOC in pool i at depth z, (gC m^{-3}) IN_{DOCi} the inflow of carbon to that pool (gCm^{-3}d^{-1}), k_i the decomposition rate of that pool (d^{-1}), Φ the temperature dependent rate modifier for DOC decomposition and $Diff$ the diffusion coefficient (m^{2}yr^{-1}). The vertical diffusion of DOC in non-permafrost soils represented here (that is, the non-cryoturbated component) appears to be consistent with recent studies reporting an increased retention of DOC in the deepening active layer of organic soils (Zhang et al., 2017). This vertical translocation of organic carbon, whether in solid/liquid phase appears to be an important component of the high rates of SOC buildup observed at depth in deep permafrost soils.

2.11 Priming (Fig. 1m)

MICT-L also incorporates a scheme for the 'priming' of organic matter decomposition, a process in which the relative stability of SOC is impacted by the intrusion of or contact with SOC of greater reactivity, resulting in enhanced rates of decomposition. This was first introduced by Guenet et al. (2016) and updated in Guenet et al. (2018). This process has shown itself to be of potentially large significance for SOC stocks and their respiration in high latitude regions, in empirical in situ and soil incubation studies (De Baets et al., 2016; Walz et al., 2017; Wild et al., 2014, 2016; Zhang et al., 2017), as well as modelling exercises (Guenet et al., 2018). Here, priming of a given soil pool is represented through the decomposition of soil carbon ($dSOC/dt$) by the following equation :

$$(6) \quad \frac{dSOC}{dt} = IN_{SOC} - k * (1 - e^{-c*FOC}) * SOC * \Theta * \phi * \gamma$$

Where IN_{SOC} is the carbon input to that pool, k is the SOC decomposition rate (1/dt), FOC (Kg) is a stock of matter interacting with this SOC pool to produce priming, c is a parameter controlling this interaction, SOC is the SOC reservoir (Kg), and θ, Φ and γ the zero-dimensional moisture, temperature and soil texture rate modifiers that modulate decomposition in the code, and are originally determined by the CENTURY formulation (Parton et al., 1987) and subsequently re-estimated to include priming in Guenet et al., (2016, 2018)."
.. The variable FOC ('fresh organic carbon') is an umbrella term used for specifying all of the carbon pools which together constitute that carbon which is considered potential priming donor material –ie. more labile – to a given receptor carbon pool. Thus, for the slow soil carbon pool FOC incorporates the active soil carbon pool plus the above and below ground structural and metabolic litter pools, because these pools are donors to the slow pool, and considered to accelerate its turnover through priming. Importantly, previous studies with priming in ORCHIDEE employed this scheme on a version which resolves neither the vertical discretisation of the soil column nor the explicit vertical diffusion processes presented here. This is potentially significant, since the vertical diffusion of relatively reactive matter may strongly impact (accelerate) the decomposition of low reactivity matter in the deeper non-frozen horizons of high latitude soils, while the explicit discretisation of the soil column is a significant improvement in terms of the accuracy of process-representation within the column

16

773 itself.
774
775 Other carbon-relevant schemes included in MICT-L are: A prognostic fire routine
776 (SPITFIRE), calibrated for the trunk version of ORCHIDEE (Yue et al., 2016) is available
777 in our code but not activated in the simulations conducted here. As a result, we do not
778 simulate the ~13% of Arctic riverine DOC attributed to biomass burning by Myers-Pigg
779 et al. (2015), or the ~8% of DOC discharge to the Arctic Ocean from the same source
780 (Stubbins et al., 2017). Likewise, a crop harvest module consistent with that in
781 ORCHIDEE-MICT exists in MICT-L but remains deactivated for our simulations.
782
783 A module introduced in the last version of ORCHIDEE-MICT (Guimberteau et al., 2018),
784 in which the soil thermal transfer and porosity and moisture are strongly affected by
785 SOC concentration, is deactivated here, because it is inconsistent with the new DOC
786 scheme. Specifically, while carbon is conserved in both MICT and MICT-L soil schemes,
787 MICT-L introduces a new reservoir into which part of the total organic carbon in the soil
788 –the DOC –must now go. This then lowers the SOC concentration being read by this
789 thermix module, causing significant model artefact in soil thermodynamics and
790 hydrology in early exploratory simulations. Ensuring compatibility of this routine with
791 the DOC scheme will be a focal point of future developments in MICT-L. Other processes
792 being developed for ORCHIDEE-MICT, including a high latitude peat formation (Qiu et
793 al., 2018), methane production and microbial heat generating processes that are being
794 optimised and calibrated, are further pending additions to this particular branch of the
795 ORCHIDEE-MICT series.
796
797 **3 Soil Carbon Spinup and Simulation Protocol**
798
799 The soil carbon spinup component of ORCHIDEE, which is available to both its trunk and
800 MICT branches, was omitted from this first version of MICT-L, owing to the code burden
801 required for ensuring compatibility with the soil carbon scheme in MICT-L. However,
802 because we are simulating high latitude permafrost regions, having a realistic soil
803 carbon pool at the outset of the simulations is necessary if we are to untangle the
804 dynamics of SOC and DOC with a changing environment. Because the soil carbon spinup
805 in ORCHIDEE-MICT is normally run over more than 10,000 years (Guimberteau et al.,
806 2108), and because running MICT-L for this simulation period in its normal, non-spinup
807 simulation mode would impose an unreasonable burden on computing resources, here
808 we directly force the soil carbon output from a MICT spinup directly into the restart file
809 of a MICT-L simulation.
810
811 A 20,000 year spinup loop over 1961-1990 (these years chosen to mimic coarsely
812 warmer mid-Holocene climate) -forced by GSWP-3 climatology, whose configuration
813 derives directly from that used in Guimberteau et al. (2018), was thus used to replace
814 the three soil carbon pool values from a 1-year MICT-L simulation to set their initial
815 values. A conversion of this soil carbon from volumetric to areal units was applied,
816 owing to different read/write standards in ORCHILEAK versus ORCHIDEE-MICT. This
817 artificially imposed, MICT-derived SOC stock would then have to be exposed to MICT-L
818 code, whose large differences in soil carbon module architecture as compared to MICT,
819 would drive a search for new equilibrium soil carbon stocks.
820
821 Due to the long residence times of the passive SOC pool, reaching full equilibrium for it

822 requires a simulation length on the order of 20,000y –again an overburden. As we are
823 interested primarily in DOC in this study, which derives mostly from the Active and Slow
824 SOC pools, the model was run until these two pools reached a quasi-steady state
825 equilibria (Part 2 Supplement, Fig. S1). This was done by looping over the same 30 year
826 cycle (1901-1930) of climate forcing data from GSWP-3 during the pre-industrial period
827 (Table 1) and the first year (1901) of a prescribed vegetation map (ESA CCI Land Cover
828 Map, Bontemps et al., (2013)) –to ensure equilibrium of DOC, dissolved CO_2 and Active
829 and Slow SOC pools is driven not just by a single set of environmental factors in one year
830 –for a total of 400 years. The parameter configuration adhered as close as possible to
831 that used in the original ORCHIDEE-MICT spinup simulations, to avoid excessive
832 equilibrium drift from the original SOC state (Fig. 3).

4 Conclusion

836 This first part of a two-part study has described a new branch of the high latitude
837 version of ORCHIDEE-MICT land surface model, in which the production, transport and
838 transformation of DOC and dissolved CO_2 in soils and along the inland water network of
839 explicitly-represented northern permafrost regions has been implemented for the first
840 time. Novel processes with respect to ORCHIDEE-MICT include the discretisation of
841 litter inputs to the soil column, the production of DOC and $CO_{2(aq.)}$ from organic matter
842 and decomposition, respectively, transport of DOC into the river routing network and its
843 potential mineralisation to $CO_{2(aq.)}$ in the water column, as well as subsequent evasion
844 from the water surface to the atmosphere. In addition, an improved floodplains
845 representation has been implemented which allows for the hydrologic cycling of DOC
846 and CO_2 in these inundated areas. In addition to descriptions of these processes, this
847 paper outlines the protocols and configuration adopted for simulations using this new
848 model that will be used for its evaluation over the Lena river basin in the second part of
849 this study.

Code and data availability

851 The source code for ORCHIDEE MICT-LEAK revision 5459 is available via
852 http://forge.ipsl.jussieu.fr/orchidee/wiki/GroupActivities/CodeAvalaibilityPublication/
853 ORCHIDEE_gmd-2018-MICT-LEAK_r5459

856 Primary data and scripts used in the analysis and other supplementary information that
857 may be useful in reproducing the author's work can be obtained by contacting the
858 corresponding author.

860 This software is governed by the CeCILL license under French law and abiding by the
861 rules of distribution of free software. You can use, modify and/or redistribute the
862 software under the terms of the CeCILL license as circulated by CEA, CNRS and INRIA at
863 the following URL: http://www.cecill.info.

Authors' contribution

866 SB coded this model version, conducted the simulations and wrote the main body of the
867 paper. RL gave consistent input to the coding process and made numerous code
868 improvements and bug fixes. BG advised on the inclusion of priming processes in the
869 model and advised on the study design and model configuration; DZ gave input on the
870 modelled soil carbon processes and model configuration. MG, AT and AD contributed to

improvements in hydrological representation and floodplain forcing data. PC oversaw all developments leading to the publication of this study. All authors contributed to suggestions regarding the final content of the study.

Competing interests

The authors declare no competing financial interests.

References:

Aitkenhead-Peterson, J. A., McDowell, W. H. and Neff, J. C.: Sources, Production, and Regulation of Allochthonous Dissolved Organic Matter Inputs to Surface Waters, in Aquatic Ecosystems., 2003.

De Baets, S., Van de Weg, M. J., Lewis, R., Steinberg, N., Meersmans, J., Quine, T. A., Shaver, G. R. and Hartley, I. P.: Investigating the controls on soil organic matter decomposition in tussock tundra soil and permafrost after fire, Soil Biol. Biochem., doi:10.1016/j.soilbio.2016.04.020, 2016.

Bardy, M., Derenne, S., Allard, T., Benedetti, M. F. and Fritsch, E.: Podzolisation and exportation of organic matter in black waters of the Rio Negro (upper Amazon basin, Brazil), Biogeochemistry, doi:10.1007/s10533-010-9564-9, 2011.

Bauch, D., Hölemann, J. A., Nikulina, A., Wegner, C., Janout, M. A., Timokhov, L. A. and Kassens, H.: Correlation of river water and local sea-ice melting on the Laptev Sea shelf (Siberian Arctic), J. Geophys. Res. Ocean., doi:10.1002/jgrc.20076, 2013.

Berezovskaya, S., Yang, D. and Hinzman, L.: Long-term annual water balance analysis of the Lena River, Glob. Planet. Change, doi:10.1016/j.gloplacha.2004.12.006, 2005.

Bergkvist, B. O. and Folkeson, L.: Soil acidification and element fluxes of a Fagus sylvatica forest as influenced by simulated nitrogen deposition, Water, Air, Soil Pollut., doi:10.1007/BF00482753, 1992.

Bogard, M. J., Kuhn, C. D., Johnston, S. E., Striegl, R. G., Holtgrieve, G. W., Dornblaser, M. M., Spencer, R. G. M., Wickland, K. P. and Butman, D. E.: Negligible cycling of terrestrial carbon in many lakes of the arid circumpolar landscape, Nat. Geosci., doi:10.1038/s41561-019-0299-5, 2019.

Bontemps, S., Defourny, P., Radoux, J., Van Bogaert, E., Lamarche, C., Achard, F., Mayaux, P., Boettcher, M., Brockmann, C., Kirches, G., Zülkhe, M., Kalogirou, V., Seifert, F. . and Arino, O.: Consistent global land cover maps for climate modelling communities: current achievements of the ESA' and cover CCI, in ESA Living Planet Symposium 2013., 2013.

Camino-Serrano, M., Gielen, B., Luyssaert, S., Ciais, P., Vicca, S., Guenet, B., Vos, B. De, Cools, N., Ahrens, B., Altaf Arain, M., Borken, W., Clarke, N., Clarkson, B., Cummins, T., Don, A., Pannatier, E. G., Laudon, H., Moore, T., Nieminen, T. M., Nilsson, M. B., Peichl, M., Schwendenmann, L., Siemens, J. and Janssens, I.: Linking variability in soil solution

920   dissolved organic carbon to climate, soil type, and vegetation type, Global Biogeochem.
921   Cycles, doi:10.1002/2013GB004726, 2014.
922   Camino-Serrano, M., Guenet, B., Luyssaert, S., Ciais, P., Bastrikov, V., De Vos, B., Gielen, B.,
923   Gleixner, G., Jornet-Puig, A., Kaiser, K., Kothawala, D., Lauerwald, R., Peñuelas, J.,
924   Schrumpf, M., Vicca, S., Vuichard, N., Walmsley, D. and Janssens, I. A.: ORCHIDEE-SOM:
925   Modeling soil organic carbon (SOC) and dissolved organic carbon (DOC) dynamics along
926   vertical soil profiles in Europe, Geosci. Model Dev., doi:10.5194/gmd-11-937-2018,
927   2018.
928   Cauwet, G. and Sidorov, I.: The biogeochemistry of Lena River: Organic carbon and
929   nutrients distribution, in Marine Chemistry., 1996.
930   Clarke, N., Wu, Y. and Strand, L. T.: Dissolved organic carbon concentrations in four
931   Norway spruce stands of different ages, Plant Soil, doi:10.1007/s11104-007-9384-4,
932   2007.
933   Cory, R. M., Ward, C. P., Crump, B. C. and Kling, G. W.: Sunlight controls water column
934   processing of carbon in arctic fresh waters, Science (80-.).,
935   doi:10.1126/science.1253119, 2014.
936   D'Orgeval, T., Polcher, J. and De Rosnay, P.: Sensitivity of the West African hydrological
937   cycle in ORCHIDEE to infiltration processes, Hydrol. Earth Syst. Sci., doi:10.5194/hess-
938   12-1387-2008, 2008.
939   DeLuca, T. H. and Boisvenue, C.: Boreal forest soil carbon: Distribution, function and
940   modelling, Forestry, doi:10.1093/forestry/cps003, 2012.
941   Denfeld, B., Frey, K. and Sobczak, W.: Summer CO 2 evasion from streams and rivers in
942   the Kolyma River basin, north-east Siberia, Polar …, doi:10.3402/polar.v32i0.19704,
943   2013.
944   Dery, S. J., Stadnyk, T. A., MacDonald, M. K. and Gauli-Sharma, B.: Recent trends and
945   variability in river discharge across northern Canada, Hydrol. Earth Syst. Sci.,
946   doi:10.5194/hess-20-4801-2016, 2016.
947   Drake, T. W., Wickland, K. P., Spencer, R. G. M., McKnight, D. M. and Striegl, R. G.: Ancient
948   low–molecular-weight organic acids in permafrost fuel rapid carbon dioxide production
949   upon thaw, Proc. Natl. Acad. Sci., doi:10.1073/pnas.1511705112, 2015.
950   Ducharne, A., Golaz, C., Leblois, E., Laval, K., Polcher, J., Ledoux, E. and De Marsily, G.:
951   Development of a high resolution runoff routing model, calibration and application to
952   assess runoff from the LMD GCM, J. Hydrol., doi:10.1016/S0022-1694(03)00230-0,
953   2003.
954   Findlay, H. S., Gibson, G., Kędra, M., Morata, N., Orchowska, M., Pavlov, A. K., Reigstad, M.,
955   Silyakova, A., Tremblay, J.-É., Walczowski, W., Weydmann, A. and Logvinova, C.:
956   Responses in Arctic marine carbon cycle processes: conceptual scenarios and
957   implications for ecosystem function, Polar Res., doi:10.3402/polar.v34.24252, 2015.
958   Fluet-Chouinard, E., Lehner, B., Rebelo, L. M., Papa, F. and Hamilton, S. K.: Development
959   of a global inundation map at high spatial resolution from topographic downscaling of
960   coarse-scale remote sensing data, Remote Sens. Environ., doi:10.1016/j.rse.2014.10.015,
961   2015.
962   Frey, K. E. and McClelland, J. W.: Impacts of permafrost degradation on arctic river
963   biogeochemistry, Hydrol. Process., doi:10.1002/hyp.7196, 2009.
964   Fröberg, M., Berggren, D., Bergkvist, B., Bryant, C. and Mulder, J.: Concentration and
965   fluxes of dissolved organic carbon (DOC) in three Norway spruce stands along a climatic
966   gradient in Sweden, Biogeochemistry, doi:10.1007/s10533-004-0564-5, 2006.
967   Gouttevin, I., Menegoz, M., Dominé, F., Krinner, G., Koven, C., Ciais, P., Tarnocai, C. and
968   Boike, J.: How the insulating properties of snow affect soil carbon distribution in the

969   continental pan-Arctic area, J. Geophys. Res. Biogeosciences,
970   doi:10.1029/2011JG001916, 2012.
971   Graham, D. E., Wallenstein, M. D., Vishnivetskaya, T. A., Waldrop, M. P., Phelps, T. J.,
972   Pfiffner, S. M., Onstott, T. C., Whyte, L. G., Rivkina, E. M., Gilichinsky, D. A., Elias, D. A.,
973   MacKelprang, R., Verberkmoes, N. C., Hettich, R. L., Wagner, D., Wullschleger, S. D. and
974   Jansson, J. K.: Microbes in thawing permafrost: The unknown variable in the climate
975   change equation, ISME J., doi:10.1038/ismej.2011.163, 2012.
976   Guenet, B., Moyano, F. E., Peylin, P., Ciais, P. and Janssens, I. A.: Towards a representation
977   of priming on soil carbon decomposition in the global land biosphere model ORCHIDEE
978   (version 1.9.5.2), Geosci. Model Dev., doi:10.5194/gmd-9-841-2016, 2016.
979   Guenet, B., Camino-Serrano, M., Ciais, P., Tifafi, M., Maignan, F., Soong, J. L. and Janssens,
980   I. A.: Impact of priming on global soil carbon stocks, Glob. Chang. Biol.,
981   doi:10.1111/gcb.14069, 2018.
982   Guimberteau, M., Drapeau, G., Ronchail, J., Sultan, B., Polcher, J., Martinez, J. M., Prigent,
983   C., Guyot, J. L., Cochonneau, G., Espinoza, J. C., Filizola, N., Fraizy, P., Lavado, W., De
984   Oliveira, E., Pombosa, R., Noriega, L. and Vauchel, P.: Discharge simulation in the sub-
985   basins of the Amazon using ORCHIDEE forced by new datasets, Hydrol. Earth Syst. Sci.,
986   doi:10.5194/hess-16-911-2012, 2012.
987   Guimberteau, M., Zhu, D., Maignan, F., Huang, Y., Yue, C., Dantec-N d lec, S., Ottl, C., Jornet-
988   Puig, A., Bastos, A., Laurent, P., Goll, D., Bowring, S., Chang, J., Guenet, B., Tifafi, M., Peng,
989   S., Krinner, G., Ducharne, A. s., Wang, F., Wang, T., Wang, X., Wang, Y., Yin, Z., Lauerwald,
990   R., Joetzjer, E., Qiu, C., Kim, H. and Ciais, P.: ORCHIDEE-MICT (v8.4.1), a land surface
991   model for the high latitudes: model description and validation, Geosci. Model Dev.,
992   doi:10.5194/gmd-11-121-2018, 2018.
993   Hastie, A., Lauerwald, R., Weyhenmeyer, G., Sobek, S., Verpoorter, C. and Regnier, P.: CO2
994   evasion from boreal lakes: Revised estimate, drivers of spatial variability, and future
995   projections, Glob. Chang. Biol., doi:10.1111/gcb.13902, 2018.
996   Heim, B., Abramova, E., Doerffer, R., Günther, F., Hölemann, J., Kraberg, A., Lantuit, H.,
997   Loginova, A., Martynov, F., Overduin, P. P. and Wegner, C.: Ocean colour remote sensing
998   in the southern laptev sea: Evaluation and applications, Biogeosciences, doi:10.5194/bg-
999   11-4191-2014, 2014.
1000   Hollesen, J., Matthiesen, H., Møller, A. B. and Elberling, B.: Permafrost thawing in organic
1001   Arctic soils accelerated by ground heat production, Nat. Clim. Chang.,
1002   doi:10.1038/nclimate2590, 2015.
1003   Holmes, R. M., McClelland, J. W., Peterson, B. J., Tank, S. E., Bulygina, E., Eglinton, T. I.,
1004   Gordeev, V. V., Gurtovaya, T. Y., Raymond, P. A., Repeta, D. J., Staples, R., Striegl, R. G.,
1005   Zhulidov, A. V. and Zimov, S. A.: Seasonal and Annual Fluxes of Nutrients and Organic
1006   Matter from Large Rivers to the Arctic Ocean and Surrounding Seas, Estuaries and
1007   Coasts, doi:10.1007/s12237-011-9386-6, 2012.
1008   Hugelius, G., Bockheim, J. G., Camill, P., Elberling, B., Grosse, G., Harden, J. W., Johnson, K.,
1009   Jorgenson, T., Koven, C. D., Kuhry, P., Michaelson, G., Mishra, U., Palmtag, J., Ping, C.-L.,
1010   O'Donnell, J., Schirrmeister, L., Schuur, E. A. G., Sheng, Y., Smith, L. C., Strauss, J. and Yu, Z.:
1011   A new data set for estimating organic carbon storage to 3m depth in soils of the
1012   northern circumpolar permafrost region, EARTH Syst. Sci. DATA, doi:10.5194/essd-5-
1013   393-2013, 2013.
1014   Hugelius, G., Strauss, J., Zubrzycki, S., Harden, J. W., Schuur, E. A. G., Ping, C. L.,
1015   Schirrmeister, L., Grosse, G., Michaelson, G. J., Koven, C. D., O'Donnell, J. A., Elberling, B.,
1016   Mishra, U., Camill, P., Yu, Z., Palmtag, J. and Kuhry, P.: Estimated stocks of circumpolar
1017   permafrost carbon with quantified uncertainty ranges and identified data gaps,

Biogeosciences, doi:10.5194/bg-11-6573-2014, 2014.

Jakobsson, M.: Hypsometry and volume of the Arctic Ocean and its constituent seas, Geochemistry, Geophys. Geosystems, doi:10.1029/2001GC000302, 2002.

Janout, M., Hölemann, J., Juhls, B., Krumpen, T., Rabe, B., Bauch, D., Wegner, C., Kassens, H. and Timokhov, L.: Episodic warming of near-bottom waters under the Arctic sea ice on the central Laptev Sea shelf, Geophys. Res. Lett., doi:10.1002/2015GL066565, 2016.

Jasechko, S., Kirchner, J. W., Welker, J. M. and McDonnell, J. J.: Substantial proportion of global streamflow less than three months old, Nat. Geosci., doi:10.1038/ngeo2636, 2016.

Kicklighter, D. W., Hayes, D. J., Mcclelland, J. W., Peterson, B. J., Mcguire, A. D. and Melillo, J. M.: Insights and issues with simulating terrestrial DOC loading of Arctic river networks, Ecol. Appl., doi:10.1890/11-1050.1, 2013.

Koven, C., Friedlingstein, P., Ciais, P., Khvorostyanov, D., Krinner, G. and Tarnocai, C.: On the formation of high-latitude soil carbon stocks: Effects of cryoturbation and insulation by organic matter in a land surface model, Geophys. Res. Lett., doi:10.1029/2009GL040150, 2009.

Koven, C. D., Riley, W. J., Subin, Z. M., Tang, J. Y., Torn, M. S., Collins, W. D., Bonan, G. B., Lawrence, D. M. and Swenson, S. C.: The effect of vertically resolved soil biogeochemistry and alternate soil C and N models on C dynamics of CLM4, Biogeosciences, doi:10.5194/bg-10-7109-2013, 2013.

Koven, C. D., Schuur, E. A. G., Schädel, C., Bohn, T. J., Burke, E. J., Chen, G., Chen, X., Ciais, P., Grosse, G., Harden, J. W., Hayes, D. J., Hugelius, G., Jafarov, E. E., Krinner, G., Kuhry, P., Lawrence, D. M., MacDougall, A. H., Marchenko, S. S., McGuire, A. D., Natali, S. M., Nicolsky, D. J., Olefeldt, D., Peng, S., Romanovsky, V. E., Schaefer, K. M., Strauss, J., Treat, C. C. and Turetsky, M.: A simplified, data-constrained approach to estimate the permafrost carbon-climate feedback, Philos. Trans. R. Soc. A Math. Phys. Eng. Sci., doi:10.1098/rsta.2014.0423, 2015.

Krinner, G., Viovy, N., de Noblet-Ducoudré, N., Ogée, J., Polcher, J., Friedlingstein, P., Ciais, P., Sitch, S. and Prentice, I. C.: A dynamic global vegetation model for studies of the coupled atmosphere-biosphere system, Global Biogeochem. Cycles, doi:10.1029/2003GB002199, 2005.

Kunkel, K. E., Robinson, D. A., Champion, S., Yin, X., Estilow, T. and Frankson, R. M.: Trends and Extremes in Northern Hemisphere Snow Characteristics, Curr. Clim. Chang. Reports, doi:10.1007/s40641-016-0036-8, 2016.

Kutscher, L., Mörth, C. M., Porcelli, D., Hirst, C., Maximov, T. C., Petrov, R. E. and Andersson, P. S.: Spatial variation in concentration and sources of organic carbon in the Lena River, Siberia, J. Geophys. Res. Biogeosciences, doi:10.1002/2017JG003858, 2017.

Lammers, R. B., Pundsack, J. W. and Shiklomanov, A. I.: Variability in river temperature, discharge, and energy flux from the Russian pan-Arctic landmass, J. Geophys. Res. Biogeosciences, doi:10.1029/2006JG000370, 2007.

Lauerwald, R., Regnier, P., Camino-Serrano, M., Guenet, B., Guimberteau, M., Ducharne, A., Polcher, J. and Ciais, P.: ORCHILEAK (revision 3875): A new model branch to simulate carbon transfers along the terrestrial-aquatic continuum of the Amazon basin, Geosci. Model Dev., doi:10.5194/gmd-10-3821-2017, 2017.

Lee, H., Swenson, S. C., Slater, A. G. and Lawrence, D. M.: Effects of excess ground ice on projections of permafrost in a warming climate, Environ. Res. Lett., doi:10.1088/1748-9326/9/12/124006, 2014.

Lindroos, A. J., Derome, J., Derome, K. and Smolander, A.: The effect of scots pine, norway spruce and silver birch on the chemical composition of stand throughfall and upper soil percolation water in northern Finland, Boreal Environ. Res., 2011.

MacKelprang, R., Waldrop, M. P., Deangelis, K. M., David, M. M., Chavarria, K. L., Blazewicz, S. J., Rubin, E. M. and Jansson, J. K.: Metagenomic analysis of a permafrost microbial community reveals a rapid response to thaw, Nature, doi:10.1038/nature10576, 2011.

Mann, P. J., Eglinton, T. I., McIntyre, C. P., Zimov, N., Davydova, A., Vonk, J. E., Holmes, R. M. and Spencer, R. G. M.: Utilization of ancient permafrost carbon in headwaters of Arctic fluvial networks, Nat. Commun., doi:10.1038/ncomms8856, 2015.

Manning, R.: On the Flow of Water in Open Channels and Pipes, Trans. Inst. Civ. Eng. Irel., doi:10.1021/bi2010619, 1891.

Manzoni, S., Taylor, P., Richter, A., Porporato, A. and Ågren, G. I.: Environmental and stoichiometric controls on microbial carbon-use efficiency in soils, New Phytol., doi:10.1111/j.1469-8137.2012.04225.x, 2012.

McClelland, J. W., Holmes, R. M., Dunton, K. H. and Macdonald, R. W.: The Arctic Ocean Estuary, Estuaries and Coasts, doi:10.1007/s12237-010-9357-3, 2012.

McClelland, J. W., Holmes, R. M., Peterson, B. J., Raymond, P. A., Striegl, R. G., Zhulidov, A. V., Zimov, S. A., Zimov, N., Tank, S. E., Spencer, R. G. M., Staples, R., Gurtovaya, T. Y. and Griffin, C. G.: Particulate organic carbon and nitrogen export from major Arctic rivers, Global Biogeochem. Cycles, doi:10.1002/2015GB005351, 2016.

McGuire, A. D., Anderson, L. G., Christensen, T. R., Dallimore, S., Guo, L., Hayes, D. J., Heimann, M., Lorenson, T. D., Macdonald, R. W. and Roulet, N.: Sensitivity of the carbon cycle in the Arctic to climate change, Ecol. Monogr., doi:10.1890/08-2025.1, 2009.

Messager, M. L., Lehner, B., Grill, G., Nedeva, I. and Schmitt, O.: Estimating the volume and age of water stored in global lakes using a geo-statistical approach, Nat. Commun., doi:10.1038/ncomms13603, 2016.

Mudryk, L. R., Derksen, C., Kushner, P. J. and Brown, R.: Characterization of Northern Hemisphere snow water equivalent datasets, 1981-2010, J. Clim., doi:10.1175/JCLI-D-15-0229.1, 2015.

Myers-Pigg, A. N., Louchouarn, P., Amon, R. M. W., Prokushkin, A., Pierce, K. and Rubtsov, A.: Labile pyrogenic dissolved organic carbon in major Siberian Arctic rivers: Implications for wildfire-stream metabolic linkages, Geophys. Res. Lett., doi:10.1002/2014GL062762, 2015.

Nachtergaele, F. et al.: The harmonized world soil database, FAO, ISRIC,ISSCAS, JRC, doi:3123, 2010.

Ngo-Duc, T., Laval, K., Ramillien, G., Polcher, J. and Cazenave, A.: Validation of the land water storage simulated by Organising Carbon and Hydrology in Dynamic Ecosystems (ORCHIDEE) with Gravity Recovery and Climate Experiment (GRACE) data, Water Resour. Res., doi:10.1029/2006WR004941, 2007.

O'Donnell, J. A., Aiken, G. R., Swanson, D. K., Panda, S., Butler, K. D. and Baltensperger, A. P.: Dissolved organic matter composition of Arctic rivers: Linking permafrost and parent material to riverine carbon, Global Biogeochem. Cycles, doi:10.1002/2016GB005482, 2016.

Oki, T., Nishimura, T. and Dirmeyer, P. A.: Assessment of annual runoff from land surface models using Total Runoff Integrating Pathways (TRIP), J. Meteorol. Soc. Japan, 1999.

Parton, W. J., Schimel, D. S., Cole, C. V. and Ojima, D. S.: Analysis of Factors Controlling Soil Organic Matter Levels in Great Plains Grasslands, Soil Sci. Soc. Am. J., 1987.

Pekel, J.-F., Cottam, A., Gorelick, N. and Belward, A. S.: Global Surface Water - Data Users Guide (JRC) High-resolution mapping of global surface water and its long-term changes, Nature, doi:10.1038/nature20584, 2016.

Peterson, B. J., Holmes, R. M., McClelland, J. W., Vörösmarty, C. J., Lammers, R. B.,

1116   Shiklomanov, A. I., Shiklomanov, I. A. and Rahmstorf, S.: Increasing river discharge to the
1117   Arctic Ocean, Science (80-.)., doi:10.1126/science.1077445, 2002.
1118   Ponomarev, E. I., Kharuk, V. I. and Ranson, K. J.: Wildfires dynamics in Siberian larch
1119   forests, Forests, doi:10.3390/f7060125, 2016.
1120   Prigent, C., Papa, F., Aires, F., Rossow, W. B. and Matthews, E.: Global inundation
1121   dynamics inferred from multiple satellite observations, 1993-2000, J. Geophys. Res.
1122   Atmos., doi:10.1029/2006JD007847, 2007.
1123   Qiu, C., Zhu, D., Ciais, P., Guenet, B., Krinner, G., Peng, S., Aurela, M., Bernhofer, C.,
1124   Brümmer, C., Bret-Harte, S., Chu, H., Chen, J., Desai, A. R., Dušek, J., Euskirchen, E. S.,
1125   Fortuniak, K., Flanagan, L. B., Friborg, T., Grygoruk, M., Gogo, S., Grünwald, T., Hansen, B.
1126   U., Holl, D., Humphreys, E., Hurkuck, M., Kiely, G., Klatt, J., Kutzbach, L., Largeron, C.,
1127   Laggoun-Défarge, F., Lund, M., Lafleur, P. M., Li, X., Mammarella, I., Merbold, L., Nilsson,
1128   M. B., Olejnik, J., Ottosson-Löfvenius, M., Oechel, W., Parmentier, F. J. W., Peichl, M., Pirk,
1129   N., Peltola, O., Pawlak, W., Rasse, D., Rinne, J., Shaver, G., Peter Schmid, H., Sottocornola,
1130   M., Steinbrecher, R., Sachs, T., Urbaniak, M., Zona, D. and Ziemblinska, K.: ORCHIDEE-
1131   PEAT (revision 4596), a model for northern peatland CO_2, water, and energy fluxes on
1132   daily to annual scales, Geosci. Model Dev., doi:10.5194/gmd-11-497-2018, 2018.
1133   Raymond, P. A., McClelland, J. W., Holmes, R. M., Zhulidov, A. V., Mull, K., Peterson, B. J.,
1134   Striegl, R. G., Aiken, G. R. and Gurtovaya, T. Y.: Flux and age of dissolved organic carbon
1135   exported to the Arctic Ocean: A carbon isotopic study of the five largest arctic rivers,
1136   Global Biogeochem. Cycles, doi:10.1029/2007GB002934, 2007.
1137   Rhein, M., Rintoul, S., Aoki, S., Campos, E., Chambers, D., Feely, R. A., Gulev, S., Johnson, G.,
1138   Josey, S., Kostianoy, A., Mauritzen, C., Roemmich, D., Talley, L., Wang, F. and IPCC:
1139   Observations: Ocean. In: Climate Change 2013: The Physical Science Basis. Contribution
1140   of Working Group I to the Fifth Assessment Report of the Intergovernmental Panel on
1141   Climate Change., 2013.
1142   Rosenqvist, L., Hansen, K., Vesterdal, L. and van der Salm, C.: Water balance in
1143   afforestation chronosequences of common oak and Norway spruce on former arable
1144   land in Denmark and southern Sweden, Agric. For. Meteorol.,
1145   doi:10.1016/j.agrformet.2009.10.004, 2010.
1146   Schuur, E. A. G., Vogel, J. G., Crummer, K. G., Lee, H., Sickman, J. O. and Osterkamp, T. E.:
1147   The effect of permafrost thaw on old carbon release and net carbon exchange from
1148   tundra, Nature, doi:10.1038/nature08031, 2009.
1149   Schuur, E. A. G., McGuire, A. D., Schädel, C., Grosse, G., Harden, J. W., Hayes, D. J., Hugelius,
1150   G., Koven, C. D., Kuhry, P., Lawrence, D. M., Natali, S. M., Olefeldt, D., Romanovsky, V. E.,
1151   Schaefer, K., Turetsky, M. R., Treat, C. C. and Vonk, J. E.: Climate change and the
1152   permafrost carbon feedback, Nature, doi:10.1038/nature14338, 2015.
1153   Selvam, B. P., Lapierre, J. F., Guillemette, F., Voigt, C., Lamprecht, R. E., Biasi, C.,
1154   Christensen, T. R., Martikainen, P. J. and Berggren, M.: Degradation potentials of
1155   dissolved organic carbon (DOC) from thawed permafrost peat, Sci. Rep.,
1156   doi:10.1038/srep45811, 2017.
1157   Serreze, M. C. and Barry, R. G.: Processes and impacts of Arctic amplification: A research
1158   synthesis, Glob. Planet. Change, doi:10.1016/j.gloplacha.2011.03.004, 2011.
1159   Shakhova, N., Semiletov, I., Sergienko, V., Lobkovsky, L., Yusupov, V., Salyuk, A.,
1160   Salomatin, A., Chernykh, D., Kosmach, D., Panteleev, G., Nicolsky, D., Samarkin, V., Joye, S.,
1161   Charkin, A., Dudarev, O., Meluzov, A. and Gustafsson, O.: The East Siberian Arctic Shelf:
1162   Towards further assessment of permafrost-related methane fluxes and role of sea ice,
1163   Philos. Trans. R. Soc. A Math. Phys. Eng. Sci., doi:10.1098/rsta.2014.0451, 2015.
1164   Smith, L. C. and Pavelsky, T. M.: Estimation of river discharge, propagation speed, and

hydraulic geometry from space: Lena River, Siberia, Water Resour. Res., doi:10.1029/2007WR006133, 2008.

Sorokin, Y. I. and Sorokin, P. Y.: Plankton and primary production in the Lena River Estuary and in the south-eastern Laptev sea, Estuar. Coast. Shelf Sci., doi:10.1006/ecss.1996.0078, 1996.

Spencer, R. G. M., Mann, P. J., Dittmar, T., Eglinton, T. I., McIntyre, C., Holmes, R. M., Zimov, N. and Stubbins, A.: Detecting the signature of permafrost thaw in Arctic rivers, Geophys. Res. Lett., doi:10.1002/2015GL063498, 2015.

Starr, M., Lindroos, A. J., Ukonmaanaho, L., Tarvainen, T. and Tanskanen, H.: Weathering release of heavy metals from soil in comparison to deposition, litterfall and leaching fluxes in a remote, boreal coniferous forest, Appl. Geochemistry, doi:10.1016/S0883-2927(02)00157-9, 2003.

Steele, M. and Ermold, W.: Loitering of the retreating sea ice edge in the Arctic Seas, J. Geophys. Res. Ocean., doi:10.1002/2015JC011182, 2015.

Stroeve, J. C., Markus, T., Boisvert, L., Miller, J. and Barrett, A.: Changes in Arctic melt season and implications for sea ice loss, Geophys. Res. Lett., doi:10.1002/2013GL058951, 2014.

Stubbins, A., Mann, P. J., Powers, L., Bittar, T. B., Dittmar, T., McIntyre, C. P., Eglinton, T. I., Zimov, N. and Spencer, R. G. M.: Low photolability of yedoma permafrost dissolved organic carbon, J. Geophys. Res. Biogeosciences, doi:10.1002/2016JG003688, 2017.

Suzuki, K., Konohira, E., Yamazaki, Y., Kubota, J., Ohata, T. and Vuglinsky, V.: Transport of organic carbon from the Mogot Experimental Watershed in the southern mountainous taiga of eastern Siberia, Hydrol. Res., doi:10.2166/nh.2006.015, 2006.

Suzuki, K., Matsuo, K., Yamazaki, D., Ichii, K., Iijima, Y., Papa, F., Yanagi, Y. and Hiyama, T.: Hydrological variability and changes in the Arctic circumpolar tundra and the three largest pan-Arctic river basins from 2002 to 2016, Remote Sens., doi:10.3390/rs10030402, 2018.

Tank, S. E., Fellman, J. B., Hood, E. and Kritzberg, E. S.: Beyond respiration: Controls on lateral carbon fluxes across the terrestrial-aquatic interface, Limnol. Oceanogr. Lett., doi:10.1002/lol2.10065, 2018.

Tarnocai, C., Canadell, J. G., Schuur, E. A. G., Kuhry, P., Mazhitova, G. and Zimov, S.: Soil organic carbon pools in the northern circumpolar permafrost retion, Global Biogeochem. Cycles, doi:Gb2023\n10.1029/2008gb003327, 2009.

Tootchi, A., Jost, A. and Ducharne, A.: Multi-source global wetland maps combining surface water imagery and groundwater constraints, Earth Syst. Sci. Data, doi:10.5194/essd-11-189-2019, 2019.

Venkiteswaran, J. J., Schiff, S. L. and Wallin, M. B.: Large carbon dioxide fluxes from headwater boreal and sub-boreal streams, PLoS One, doi:10.1371/journal.pone.0101756, 2014.

Vitousek, P. M. and Hobbie, S.: Heterotrophic nitrogen fixation in decomposing litter: Patterns and regulation, Ecology, doi:10.1890/0012-9658(2000)081[2366:HNFIDL]2.0.CO;2, 2000.

Vitousek, P. M. and Sanford, R. L.: Nutrient Cycling in Moist Tropical Forest, Ecology, doi:0.1146/annurev.es.17.110186.001033, 1986.

Van Vliet, M. T. H., Yearsley, J. R., Franssen, W. H. P., Ludwig, F., Haddeland, I., Lettenmaier, D. P. and Kabat, P.: Coupled daily streamflow and water temperature modelling in large river basins, Hydrol. Earth Syst. Sci., doi:10.5194/hess-16-4303-2012, 2012.

Van Vliet, M. T. H., Franssen, W. H. P., Yearsley, J. R., Ludwig, F., Haddeland, I.,

1214 Lettenmaier, D. P. and Kabat, P.: Global river discharge and water temperature under
1215 climate change, Glob. Environ. Chang., doi:10.1016/j.gloenvcha.2012.11.002, 2013.
1216 Vonk, J. E., Mann, P. J., Davydov, S., Davydova, A., Spencer, R. G. M., Schade, J., Sobczak, W.
1217 V., Zimov, N., Zimov, S., Bulygina, E., Eglinton, T. I. and Holmes, R. M.: High biolability of
1218 ancient permafrost carbon upon thaw, Geophys. Res. Lett., doi:10.1002/grl.50348, 2013.
1219 Vonk, J. E., Tank, S. E., Mann, P. J., Spencer, R. G. M., Treat, C. C., Striegl, R. G., Abbott, B. W.
1220 and Wickland, K. P.: Biodegradability of dissolved organic carbon in permafrost soils and
1221 aquatic systems: A meta-analysis, Biogeosciences, doi:10.5194/bg-12-6915-2015,
1222 2015a.
1223 Vonk, J. E., Tank, S. E., Bowden, W. B., Laurion, I., Vincent, W. F., Alekseychik, P., Amyot,
1224 M., Billet, M. F., Canário, J., Cory, R. M., Deshpande, B. N., Helbig, M., Jammet, M., Karlsson,
1225 J., Larouche, J., MacMillan, G., Rautio, M., Walter Anthony, K. M. and Wickland, K. P.:
1226 Reviews and Syntheses: Effects of permafrost thaw on arctic aquatic ecosystems,
1227 Biogeosciences Discuss., doi:10.5194/bgd-12-10719-2015, 2015b.
1228 Vorosmarty, C. J., Fekete, B. M., Meybeck, M. and Lammers, R. B.: Global system of rivers:
1229 Its role in organizing continental land mass and defining land-To-Ocean linkages, Global
1230 Biogeochem. Cycles, doi:10.1029/1999GB900092, 2000.
1231 Walz, J., Knoblauch, C., Böhme, L. and Pfeiffer, E. M.: Regulation of soil organic matter
1232 decomposition in permafrost-affected Siberian tundra soils - Impact of oxygen
1233 availability, freezing and thawing, temperature, and labile organic matter, Soil Biol.
1234 Biochem., doi:10.1016/j.soilbio.2017.03.001, 2017.
1235 Wang, T., Ottlé, C., Boone, A., Ciais, P., Brun, E., Morin, S., Krinner, G., Piao, S. and Peng, S.:
1236 Evaluation of an improved intermediate complexity snow scheme in the ORCHIDEE land
1237 surface model, J. Geophys. Res. Atmos., doi:10.1002/jgrd.50395, 2013.
1238 Wanninkhof, R.: Relationship between wind speed and gas exchange over the ocean
1239 revisited, Limnol. Oceanogr. Methods, doi:10.4319/lom.2014.12.351, 2014.
1240 Wanninkhof, R. H.: Relationship between wind speed and gas exchange, J. Geophys. Res.,
1241 doi:10.1029/92JC00188, 1992.
1242 Whitefield, J., Winsor, P., McClelland, J. and Menemenlis, D.: A new river discharge and
1243 river temperature climatology data set for the pan-Arctic region, Ocean Model.,
1244 doi:10.1016/j.ocemod.2014.12.012, 2015.
1245 Wickland, K. P., Waldrop, M. P., Aiken, G. R., Koch, J. C., Jorgenson, M. T. and Striegl, R. G.:
1246 Dissolved organic carbon and nitrogen release from boreal Holocene permafrost and
1247 seasonally frozen soils of Alaska, Environ. Res. Lett., doi:10.1088/1748-9326/aac4ad,
1248 2018.
1249 Wild, B., Schnecker, J., Alves, R. J. E., Barsukov, P., Bárta, J., Čapek, P., Gentsch, N., Gittel, A.,
1250 Guggenberger, G., Lashchinskiy, N., Mikutta, R., Rusalimova, O., Šantrůčková, H.,
1251 Shibistova, O., Urich, T., Watzka, M., Zrazhevskaya, G. and Richter, A.: Input of easily
1252 available organic C and N stimulates microbial decomposition of soil organic matter in
1253 arctic permafrost soil, Soil Biol. Biochem., doi:10.1016/j.soilbio.2014.04.014, 2014.
1254 Wild, B., Gentsch, N., Capek, P., Diáková, K., Alves, R. J. E., Bárta, J., Gittel, A., Hugelius, G.,
1255 Knoltsch, A., Kuhry, P., Lashchinskiy, N., Mikutta, R., Palmtag, J., Schleper, C., Schnecker, J.,
1256 Shibistova, O., Takriti, M., Torsvik, V. L., Urich, T., Watzka, M., Šantrůcková, H.,
1257 Guggenberger, G. and Richter, A.: Plant-derived compounds stimulate the decomposition
1258 of organic matter in arctic permafrost soils, Sci. Rep., doi:10.1038/srep25607, 2016.
1259 Woods, G. C., Simpson, M. J., Pautler, B. G., Lamoureux, S. F., Lafrenière, M. J. and Simpson,
1260 A. J.: Evidence for the enhanced lability of dissolved organic matter following permafrost
1261 slope disturbance in the Canadian High Arctic, Geochim. Cosmochim. Acta,
1262 doi:10.1016/j.gca.2011.08.013, 2011.

Wu, Y., Clarke, N. and Mulder, J.: Dissolved organic carbon concentrations in throughfall and soil waters at level II monitoring plots in norway: Short- and long-term variations, Water. Air. Soil Pollut., doi:10.1007/s11270-009-0073-1, 2010.

Xue, K.: Tundra soil carbon is vulnerable to rapid microbial decomposition under climatewarming, Nat. Clim. Chang., doi:10.1038/NCLIMATE2940, 2017.

Ye, B., Yang, D., Zhang, Z. and Kane, D. L.: Variation of hydrological regime with permafrost coverage over Lena Basin in Siberia, J. Geophys. Res. Atmos., doi:10.1029/2008JD010537, 2009.

Yu, Z.: Holocene carbon flux histories of the world's peatlands: Global carbon-cycle implications, Holocene, doi:10.1177/0959683610386982, 2011.

Yue, C., Ciais, P., Zhu, D., Wang, T., Peng, S. S. and Piao, S. L.: How have past fire disturbances contributed to the current carbon balance of boreal ecosystems?, Biogeosciences, doi:10.5194/bg-13-675-2016, 2016.

Zhang, K., Kimball, J. S., Mu, Q., Jones, L. A., Goetz, S. J. and Running, S. W.: Satellite based analysis of northern ET trends and associated changes in the regional water balance from 1983 to 2005, J. Hydrol., doi:10.1016/j.jhydrol.2009.09.047, 2009.

Zhang, X., Hutchings, J. A., Bianchi, T. S., Liu, Y., Arellano, A. R. and Schuur, E. A. G.: Importance of lateral flux and its percolation depth on organic carbon export in Arctic tundra soil: Implications from a soil leaching experiment, J. Geophys. Res. Biogeosciences, doi:10.1002/2016JG003754, 2017.

Zhu, D., Peng, S., Ciais, P., Zech, R., Krinner, G., Zimov, S. and Grosse, G.: Simulating soil organic carbon in yedoma deposits during the Last Glacial Maximum in a land surface model, Geophys. Res. Lett., doi:10.1002/2016GL068874, 2016.

Zubrzycki, S., Kutzbach, L., Grosse, G. and Desyatkin, A.: Organic carbon and total nitrogen stocks in soils of the Lena River Delta, Biogeosciences, doi:10.5194/bg-10-3507-2013, 2013.

Tables and Figures:

Table 1: Data type, name and sources of data files used to drive the model in the study simulations.

Data Type	Name	Source
Vegetation Map	ESA CCI Land Cover Map	Bontemps et al., 2013
Topographic Index	STN-30p	Vörösmarty et al., 2000
Stream flow direction	STN-30p	Vörösmarty et al., 2000
River surface area		Lauerwald et al., 2015
Soil texture class		Reynolds et al. 1999
Climatology	GSWP3 v0, 1 degree	http://hydro.iis.u-tokyo.ac.jp/GSWP3/
Potential floodplains	Multi-source global wetland maps	Tootchi et al., 2019
Poor soils	Harmonized World Soil Database map	Nachtergaele et al., 2010
Spinup Soil Carbon Stock	20ky ORCHIDEE-MICT soil carbon spinup	Based on config. in Guimberteau et al. (2018)
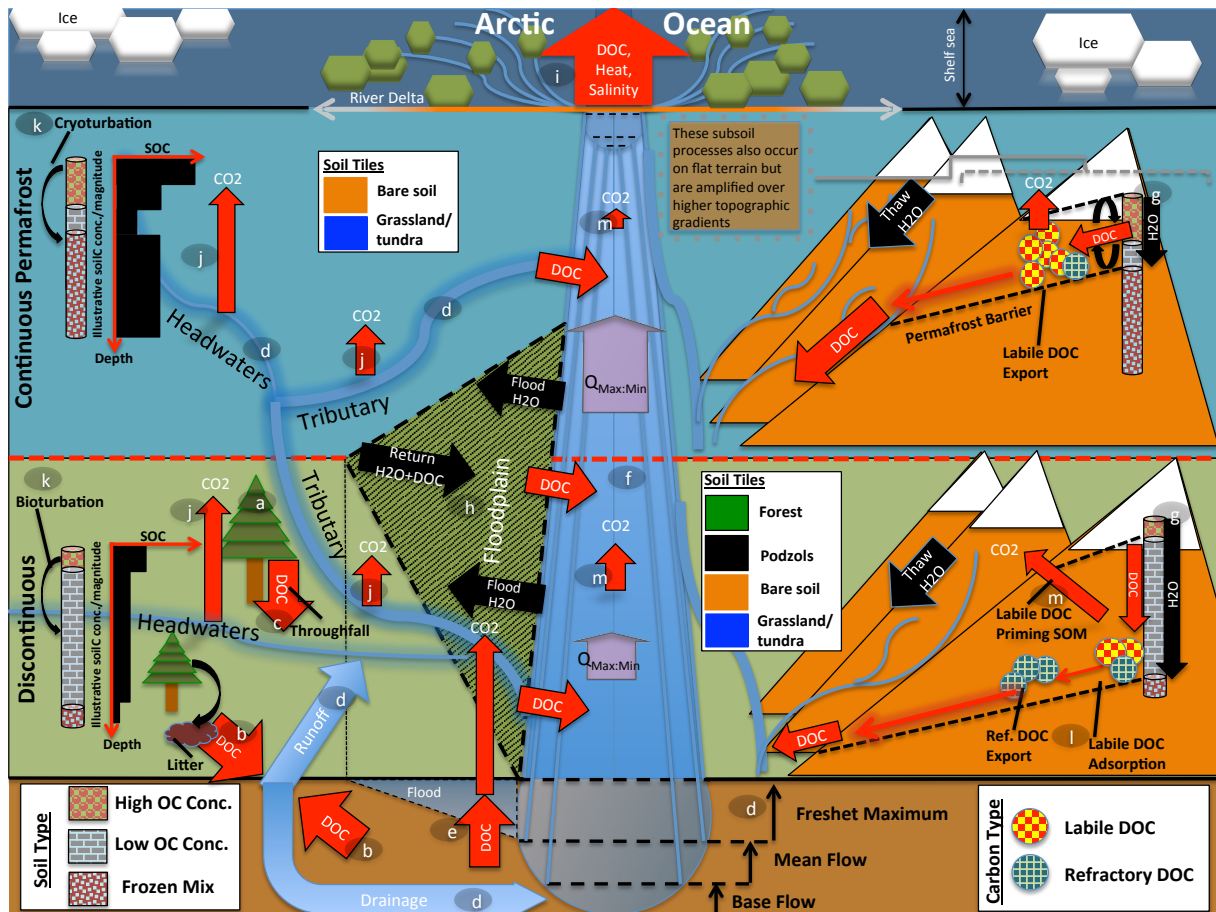
Figure 1: Cartoon diagram illustrating the landscape-scale emergent phenomena observed in high-latitude river systems that are captured by the processes represented in this model. Here, the terrestrial area is shown, in vertically-ascending order, as subsoil, discontinuous permafrost, continuous permafrost and the maritime boundary. Note that 'tributaries' in the Figure may be represented in the model by either the 'fast' or 'stream' pool, depending on their size. Representative soil types, their distributions and carbon concentrations are shown for the two permafrost zones, as well as the different dynamics occuring on 'flat' (left) and 'sloping' land (right) arising from their permafrost designation. Carbon exports from one subsystem to another are shown in red. The relative strength of the same processes ocurring in each permafrost band are indicated by relative arrow size. Note that the high CO_2 evasion in headwaters versus tributaries versus mainstem is shown here. Proposed and modelled mechanisms of soil carbon priming, adsorption and rapid metabolisation are shown. The arrows $Q_{Max:Min}$ refer to the ratio of maximum to minimum discharge at a given point in the river, the ratio indicating hydrologic volatility, whose magnitude is influenced by permafrost coverage. Soil tiles, a model construct used for modulating soil permeability and implicit/explicit decomposition, are shown to indicate the potential differences in these dynamics for the relevant permafrost zones. Note that the marine shelf sea system, as shown in the uppermost rectangle, is not simulated in this model, although our outputs can be coupled for that purpose. Letter markings mark processes of carbon flux in permafrost regions and implicitly or explicitly included in the model, and can be referred to in subsections of the Methods text. These refer to: (a) Biomass generation; (b) DOC generation and leaching; (c) Throughfall and its DOC; (d) Hydrological mobilisation of soil DOC; (e) Soil flooding; (f) Landscape routing of water and carbon; (g)

28

1325 Infiltration and topography; (h) Floodplain representation; (i) Oceanic outflow; (j)
1326 Dissolved carbon export and riverine atmospheric evasion; (k) Turbation and soil
1327 carbon with depth (e.g. (Hugelius et al., 2013; Tarnocai et al., 2009), (Koven et al.,
1328 2015)); (l) Adsorption; (m) Priming.
1329
1330
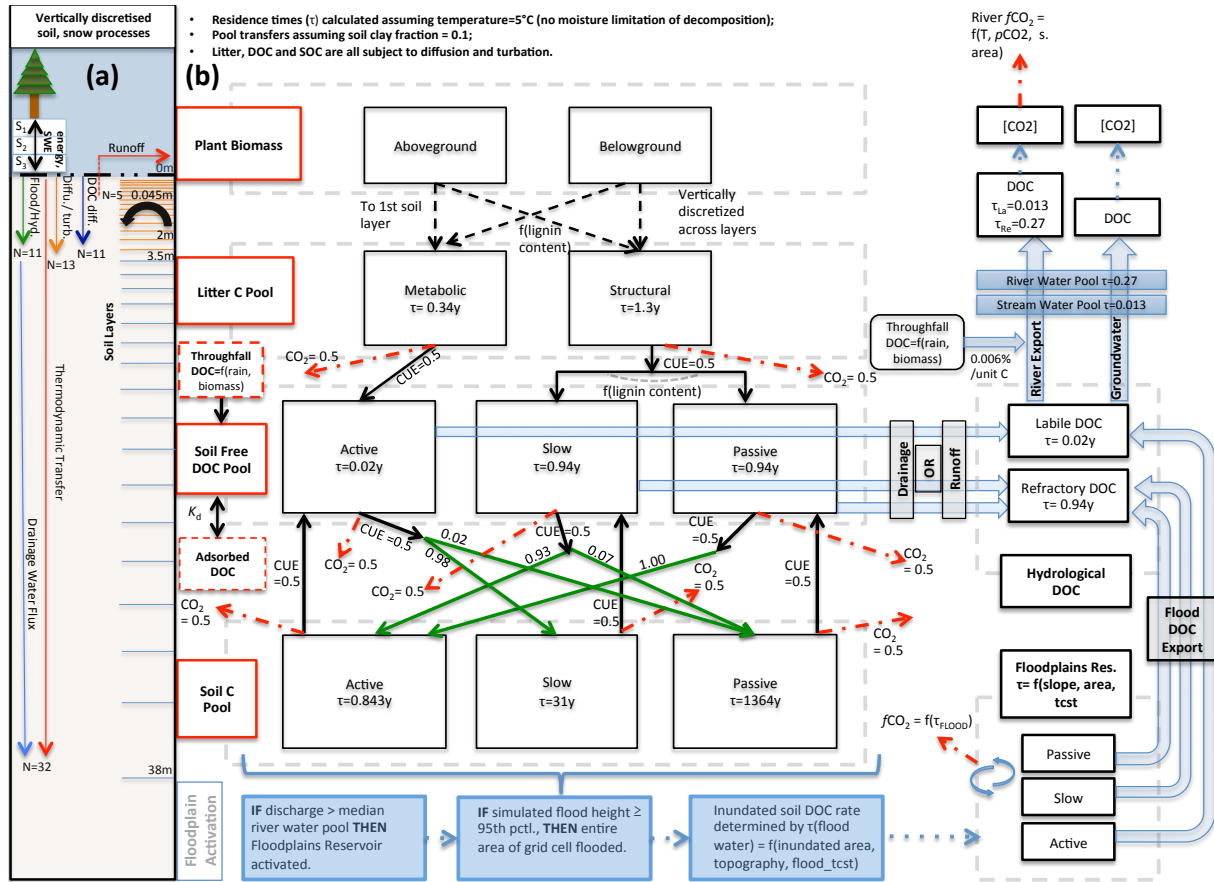
1331
1332
1333
1334 **Figure 2** :Carbon and water flux map for core DOC elements in model structure relating
1335 to DOC transport and transformation. **(a)** Summary of the differing extent of vertical
1336 discretisation of soil and snow for different processes calculated in the model.
1337 Discretisation occurs along 32 layers whose thickness increases geometrically from 0-
1338 38m. N refers to the number of layers, SWE=snow water equivalent, S_n = Snow layer n.
1339 Orange layers indicate the depth to which diffusive carbon (turbation) fluxes occur. **(b)**
1340 Conceptual map of the production, transfer and transformation of carbon in its vertical
1341 and lateral (i.e., hydrological) flux as calculated in the model. Red boxes indicate meta-
1342 reservoirs of carbon, black boxes the actual pools as they exist in the model. Black
1343 arrows indicate carbon fluxes between pools, dashed red arrows give carbon loss as CO_2,
1344 green arrows highlight the fractional distribution of DOC to SOC (no carbon loss
1345 incurred in this transfer), a feature of this model. For a given temperature (5°C) and soil
1346 clay fraction, the fractional fluxes between pools are given for each flux, while residence
1347 times for each pool (τ) are in each box. The association of carbon dynamics with the
1348 hydrological module are shown by the blue arrows. Blue coloured boxes illustrate the
1349 statistical sequence which activates the boolean floodplains module. Note that for

1350 readability, the generation and lateral flux of dissolved CO_2 is omitted from this diagram,
1351 but is described at length in the Methods section.
1352
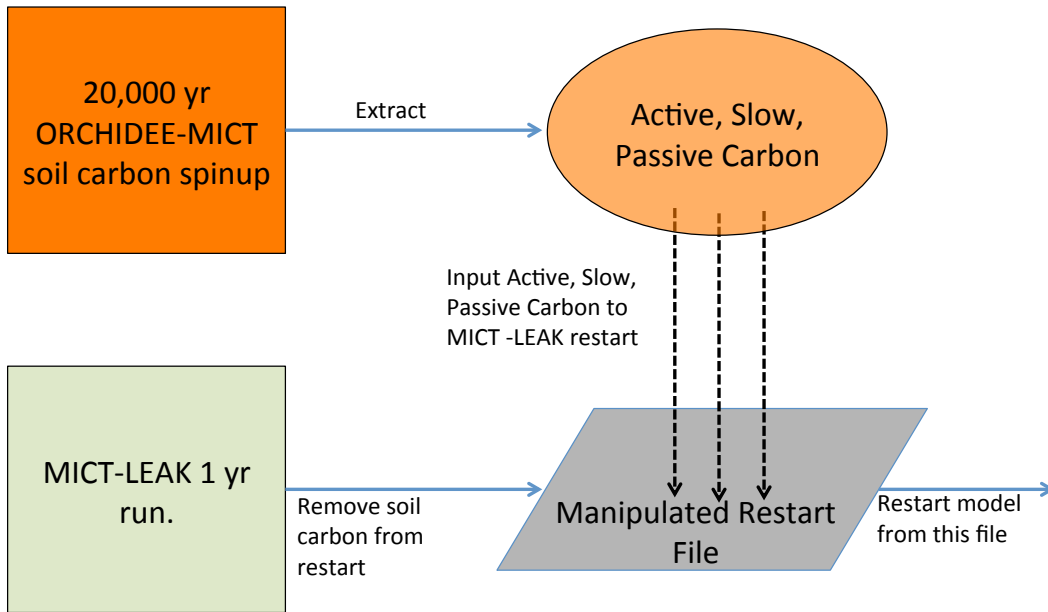
1353
1354 **Figure 3:** Flow diagram illustrating the step-wise stages required to implement the
1355 model's soil carbon stock prior to conducting transient, historical simulations.